Composite Atmospheric Environments of Jet Contrail Outbreaks for the United States

ANDREW M. CARLETON

Department of Geography, and Earth and Environmental Systems Institute, The Pennsylvania State University, University Park, Pennsylvania

DAVID J. TRAVIS

Department of Geography and Geology, University of Wisconsin—Whitewater, Whitewater, Wisconsin

KARA MASTER

College of Earth and Mineral Sciences, The Pennsylvania State University, University Park, Pennsylvania

SAJITH VEZHAPPARAMBU

Department of Geosciences, University of Missouri—Kansas City, Kansas City, Missouri

(Manuscript received 18 April 2006, in final form 17 May 2007)

ABSTRACT

The cirrus-level "condensation trails" (contrails) produced by jet aircraft are considered to influence surface climate and its recent changes. To reveal the synoptic atmospheric environments typically associated with multiple co-occurrences of contrails occurring in otherwise clear or partly cloudy skies (outbreaks) for the United States, and ultimately to assist in forecasting these events, a composite (i.e., multicase average) "synoptic climatology" at regional scales is developed for the midseason months (January, April, July, October) of 2000–02. The NCEP–NCAR reanalysis data that emphasize upper-troposphere (UT) variables are allied with manually identified outbreaks appearing on satellite Advanced Very High Resolution Radiometer digital data, using a geographic information system. The highest frequencies of outbreaks by far occur in the Midwest (32.6% of all-U.S. total), followed by the Northeast (17.6%) and Southeast (17.2%). In these regions, all of which have a high density of jet air traffic, an additional 2% cirrus cloud coverage from outbreak-related contrails is inferred. Large interannual and interseasonal variations in contrail outbreak frequencies support the role of meteorological variations. For most regions, the outbreak-associated synoptic circulation composite conditions involve UT ridging and a higher and colder tropopause than the climatological average; meridionally enhanced gradients of the UT vertical motion, located between sinking air to the east (in the ridge) and rising air to the west, in advance of a trough; similarly strong gradients of mid–upper-troposphere humidity, comprising dry air located to the east and moist air to the west; and horizontal speed shear ahead of an advancing jet stream. Notwithstanding, there is a geography (i.e., areal differentiation) to contrail outbreak environments: composites for the Northeast suggest an influence of land–sea contrasts on synoptic systems and, therefore, on contrail outbreaks. For the Northwest, there is evident a greater impact of horizontal wind shear contrasted with other regions. The synoptic climatology results are supported by the all-U.S. averages of contrail outbreak UT conditions [climate diagnostics (CDNs)] previously determined for early–mid-September periods of 1995–2001. Moreover, a comparison of these CDNs with those derived for nearby thick natural clouds, including cirrus, helps to clarify their different synoptic associations: the UT conditions typical of thick clouds represent an intensification of those associated with contrail outbreaks and include the greater upward vertical motion, moister air, and stronger westerly winds characteristic of a trough. Given the location of most contrail outbreaks downstream of multilayered cloud systems, contrails may help to extend the "natural" cirrus and cirrostratus spatial coverage.

Corresponding author address: Andrew Carleton, Department of Geography, and Earth and Environmental Systems Institute, The Pennsylvania State University, University Park, PA 16802.
E-mail: carleton@essc.psu.edu

DOI: 10.1175/2007JAMC1481.1

1. Introduction

Much debate centers on the role of jet-aircraft-generated contrails and their resulting contrail cirrus in surface climate changes at regional scales, especially for the United States and Europe (e.g., Changnon 1981; Angell 1990; Sassen 1997; Nakanishi et al. 2001; Del Guasta and Vallar 2003; Ponater et al. 2005). Recent climate trends potentially attributed to contrail formation by commercial aviation include the following: increases in high cloudiness, reduced surface receipts of solar radiation, reductions in surface diurnal temperature range (DTR), and declines in terrestrial pan evaporation (e.g., Nicodemus and McQuigg 1969; Liepert 1997; Travis and Changnon 1997; Travis et al. 2002; Matuszko 2002; Roderick and Farquhar 2002; Minnis et al. 2004; Stordal et al. 2005; Stubenrauch and Schumann 2005). A contrail–climate connection has been argued from the spatial coincidence of these trends with jet aviation attributes, particularly maxima in fuel usage, high-altitude flight-path locations, and high frequencies of contrails (Sassen 1997; Boucher 1999; Ross et al. 1999; DeGrand et al. 2000; Minnis et al. 2003; Zerefos et al. 2003; Travis et al. 2004). Temporally, many trends of increased station high cloud amount on regional and subregional scales date to around the advent of commercial jet air transportation (Machta and Carpenter 1971; Seaver and Lee 1987; Liou et al. 1990; Nakanishi et al. 2001).

Contrails are the visible condensate of water vapor emitted from aircraft engines and that sublimated from the environment (Schumann 1996; Chlond 1998). A jet engine may produce a contrail (any duration) thermodynamically according to the ambient temperature and humidity, as modified by the following factors: the water vapor emission index (Appleman 1953); aircraft flight altitude (Scorer and Davenport 1970; Sausen et al. 1998); the engine efficiency (Peters 1993; Schrader 1997; Schumann 2000) and—although it has only a minor influence—the fuel type, including its sulfur content (Busen and Schumann 1995; Schumann et al. 1996). However, the ability of contrails to persist—and potentially be significant for weather and climate—is determined by the upper-tropospheric (UT) meteorological conditions at jetliner cruise altitudes (typically between 10 and 13 km); in particular, air that is supersaturated with respect to ice (Appleman 1953; Pilié and Jiusto 1958; Grassl 1990; Hanson and Hanson 1995; Schrader 1997; Jensen et al. 1998; Sausen et al. 1998; Minnis et al. 2003; Duda et al. 2004; Schumann 2005). GCM experiments to assess the relative contributions globally of persisting contrails and aircraft water vapor emissions suggest that the contrail cirrus radiative forcing far exceeds that due to the additional water vapor for current and predicted (i.e., near future) aviation (e.g., Ponater et al. 1996; Rind et al. 1996; Penner et al. 1999). Thus, contrails and contrail cirrus likely compose the dominant contribution to radiative forcing from aircraft emissions (Penner et al. 1999; Pielke 2003; Sausen et al. 2005). Large uncertainties in the contrail net radiative forcing are related to the following factors: geographic location; the wide range of contrail optical thickness and altitude; diurnal and seasonal variations in contrail occurrence; contrail interactions with aerosols; the extent to which contrails co-occur with natural clouds, particularly cirrus; and subdaily variations in flight frequency (Myhre and Stordal 2001; Ponater et al. 2002; Meyer et al. 2002; Minnis et al. 2003, 2004; Garber et al. 2005; Palikonda et al. 2005; Stuber et al. 2006).

Although contrails and natural cirrus occur at broadly similar altitudes, differences in the cloud microphysics (e.g., particle size, particle density) are greatest for young contrails and decrease with age (Schröder et al. 2000). Thus, young contrails likely impact surface climate differently to natural cirrus (e.g., Liou et al. 1990; Gothe and Grassl 1993; Strauss et al. 1997; Duda et al. 1998; Khvorostyanov and Sassen 1998; Meerkötter et al. 1999; Penner et al. 1999). Also, UT meteorological conditions may differ between areas of persisting contrails and natural cirrus and cirrostratus clouds (Kristensson et al. 2000; Mace et al. 2006). It has been suggested that contrails may help extend the natural cirrus coverage generated by deep convection or associated with baroclinic zones (Carleton and Lamb 1986), possibly explaining at least part of the increase in high-level cloudiness observed over the United States—indeed, much of the Northern Hemisphere extratropics—in recent decades (e.g., Lee and Johnson 1985; Seaver and Lee 1987; Boucher 1999; Wylie et al. 2005).

A climatic impact of contrails likely is significant when and where: 1) they occur as multiple, rather than single, features covering a significant portion of the sky dome (i.e., in areas of high flight density); and 2) they persist for several hours, or "persistent contrails" (Minnis et al. 1998), increasing the opportunity for them to merge and form contrail cirrus (e.g., Lee 1989; Schumann and Wendling 1990; Meyer et al. 2002; Mannstein and Schumann 2005). These contrail joint criteria are met in otherwise clear or partly cloudy skies (Duda et al. 2001, 2004), and also when embedded within the natural cloud cover, including cirrus (Gierens 1996; Mannstein et al. 1999). They compose subregional-scale clusters, or outbreaks, that may cover areas exceeding 1×10^3 km^2 and persist for at least 3 h

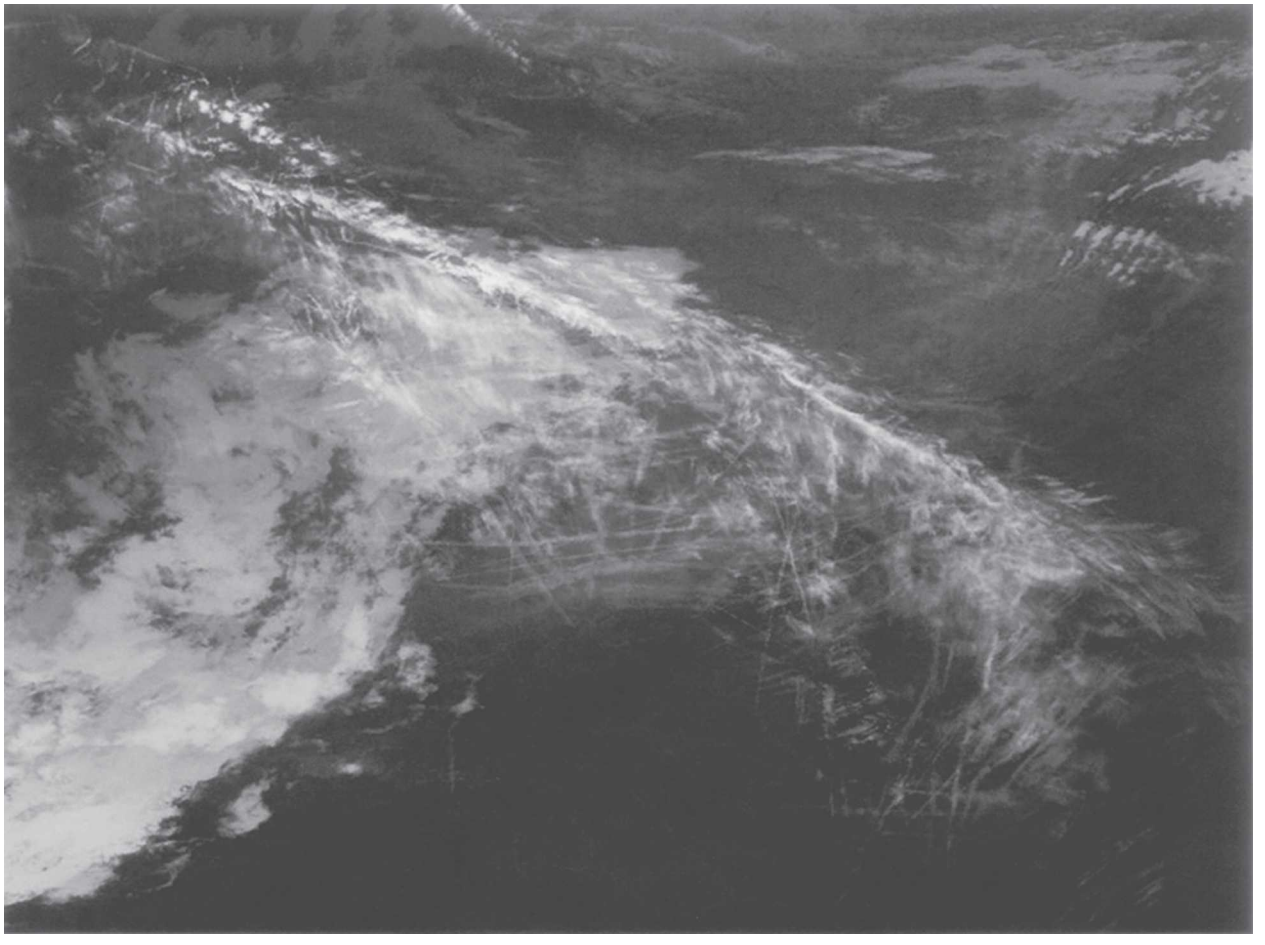

FIG. 1. AVHRR IR image for 18 Jul 2000 (1411 UTC) of a contrail outbreak in the central United States (center and lower right of image). An area of thicker low and middle clouds with some overlying cirrus and cirrostratus is located west of the outbreak (left third of image).

(Fig. 1; Bakan et al. 1994; Travis et al. 1997; Minnis et al. 1999). Because the radiative contribution of multiple contrails occurring in the presence of other clouds likely is moderated compared with those contrails in mostly clear skies (e.g., Palikonda et al. 2005), it has been argued (Liou et al. 1990; Fortuin et al. 1995; Strauss et al. 1997; Poellot et al. 1999; Minnis et al. 1999; Duda et al. 2001) that the climatic impact of the latter type is greater. Accordingly, this study focuses on contrail outbreaks occurring in otherwise clear or partly cloudy skies, and which are readily identified in satellite data using manual (i.e., visual) methods.

Determining the atmospheric conditions associated with persisting contrails and outbreaks is important for reasons in addition to their potential climatic impact, and include the military and strategic requirements of aircraft stealth (Hanson and Hanson 1998; Moss 1999; Jackson et al. 2001). Also, a consequence of the contrail climate impact is to better inform public policy debates (Williams et al. 2003; Fichter et al. 2005; Stuber et al. 2006). A major objective of current contrail forecasting methods identifies mesoscale contrail-forming (i.e., "favored") areas (CFAs) that may be either avoided or intentionally penetrated by aircraft, according to the desired impact (cf. Nicodemus and McQuigg 1969; Detwiler and Cho 1982; Detwiler and Pratt 1984; Penner et al. 1999; Travis and Carleton 2005; Schumann 2005). Most contrail prediction operational methods rely on detecting critical thresholds of UT temperature and humidity, or Schmidt–Appleman criteria (e.g., Peters 1993; Hanson and Hanson 1995, 1998; Schumann 1996; Newton et al. 1997; Jackson et al. 2001; Stuefer et al. 2005). However, these thresholds frequently are transient or occur on relatively small scales (e.g., Duda et al. 2004): they require meteorological observations at high resolutions in the horizontal, vertical, and temporal domains, such as those becoming available with the Aircraft Communication Addressing and Reporting System (ACARS; e.g., Moninger et al. 2003; Cardinali et al. 2003). Given the requirement of ice supersaturation,

the UT humidity (UTH) particularly is significant for contrail persistence (e.g., Appleman 1953; Pilié and Jiusto 1958; Freudenthaler et al. 1995; Sausen et al. 1998; Gierens et al. 2000; Vay et al. 2000; Minnis et al. 2004), yet reliable data on this variable often are not available (e.g., Elliott and Gaffen 1991; Garand et al. 1992). Information on aircraft jet fuel usage, engine efficiency, or flight frequency may be combined with a measure of the cloud-generating potential in the UT, typically moisture and temperature (Liou 1992; Sausen et al. 1998; Gierens et al. 1999; Minnis et al. 1999; Duda et al. 2005), although this method does not substitute for actual contrail observations because of the importance of synoptic meteorological conditions in contrail formation and persistence, particularly baroclinity (cf. Sassen 1997; Ross et al. 1999; DeGrand et al. 2000). Last, there can be a mismatch between model-generated analyses of UTH and the contrail cirrus cloudiness (Ovarlez et al. 2000; Palikonda et al. 2005), likely related to the requirement for ice supersaturation (Gierens et al. 2000).

Determining the spatial dependence of CFAs, at least in the first instance, uses identification of the synoptic atmospheric environments typically accompanying contrail outbreaks for a given region or subregion, and which are familiar to meteorologists (e.g., Carleton and Lamb 1986; Kästner et al. 1999). This "synoptic climatological" indexing approach (e.g., Carleton 1999; Barry and Carleton 2001, chapter 2) composites (i.e., averages) the mapped data on a number of key meteorological variables (e.g., geopotential height, air temperature, humidity, vertical motion, vector winds), or their anomalies, for multiple events [cf. the cirrus cloud climatology of the U.S. southern Great Plains, in Mace et al. (2006)]. By reducing the influence of an individual event or case, the dominant atmospheric controls that are revealed facilitate interpretation by a synoptic analyst or forecaster. Compositing does not replace the detailed study of cases (e.g., using higher-resolution data); rather, it complements these by permitting assessment of either the representativeness or uniqueness of the case under consideration. Moreover, because a range of variables important for contrail development are included, the composite method likely is superior to using forecast-model-generated fields of UTH alone. For example, Travis et al. (2004) developed a geographic information system (GIS)–based statistical model to "retro-predict" where persisting contrails and outbreaks likely would have occurred during the U.S.-wide grounding of commercial aircraft between 11 and 14 September 2001, had aviation continued unabated. The model was based upon the composite UT conditions of humidity, temperature, vertical motion, and vertical wind shear, associated with 47 contrail outbreaks identified for the 8–16 (early–mid) September periods of 1995–97 and 1999–2001, and subsequently verified as having skill for the series' central year (1998). When applied to UT meteorological analyses for the 3-day grounding period, the statistical method retrodicted CFAs showing maximum "susceptibility" in the Intermountain West and south-central United States, and in the Midwest, New England, and Florida (Travis et al. 2004, their Fig. 7). Most of these CFAs coincided with locations that experienced maximum positive departures of DTR during the grounding period, further suggesting a climatic role of contrails in reducing the contemporary-period DTR; at least, for late summer. Thus, to operationally predict the atmospheric susceptibility of persisting contrails, areas of strong potential identified using Numerical Weather Prediction (NWP) output could be further refined using higher-resolution data (e.g., from ACARS).

Given the apparent synoptic associations of contrail outbreaks, their likely significance to climate, and the need to better predict general areas of atmospheric susceptibility at regional and subregional scales, we determine the composite atmospheric environments—or "synoptic climatology"—of contrail outbreaks occurring in otherwise clear or partly cloudy skies, as revealed in satellite high-resolution imagery for the conterminous United States. The outbreaks are those identified for the midseason months (January, April, July, October) of 2000–02 from a contemporary spatial climatology of contrails derived for the conterminous United States using National Oceanic and Atmospheric Administration (NOAA) Advanced Very High Resolution Radiometer (AVHRR) images (Travis and Carleton 2005; Travis et al. 2007). Satellite observations of persistent contrails and outbreaks are superior to surface observations for the synoptic context they provide. Also, when lower clouds are present, contrails are more readily detected from space than the ground (e.g., Engelstad et al. 1992; Travis 1996a; DeGrand et al. 2000; Travis and Carleton 2005; Palikonda et al. 2005). Contrail outbreaks are particularly well depicted in high-resolution satellite data (Carleton and Lamb 1986; Minnis et al. 1998; Duda et al. 2001, 2004) given the linearity of the persisting contrails comprising them; at least, in the early stages, and their relatively low temperature in the thermal infrared (IR). Moreover, the orientations of contrails composing an outbreak frequently differ from each other as well as from any natural cirrus streamers in the area (Fig. 1); the latter tending to be aligned with the synoptic flow (Carleton and Lamb 1986; Mannstein et al. 1999). In contrast to the present study of multiple outbreak events, previous studies

FIG. 2. Regionalization of the United States used to derive the synoptic climatology of contrail outbreaks. Regions are determined from the spatial patterns of contrail frequencies indicated in previous satellite-based "climatologies" (see text).

mostly have analyzed the atmospheric conditions associated with a persisting contrail or outbreak case (e.g., Sassen et al. 2001; Langford et al. 2005; Atlas et al. 2006).

We derive the regional map patterns using National Centers for Environmental Prediction–National Center for Atmospheric Research (NCEP–NCAR) reanalysis (NNR) daily-averaged gridded data that emphasize the UT and are expressed as departures from the long-term daily means. Our use of daily-averaged data is permissible given that we are averaging spatially (i.e., over a subregion) as well as temporally (multiple events). However, when analyzing an individual outbreak, daily-averaged data would not be appropriate because the synoptic situation can change strongly within a given 24-h period. We composite the anomalies of the variables, rather than the actual daily map values, as these better indicate the departures of atmospheric fields from a climatological (long-term) normal, and permit cross-seasonal direct comparisons of CFAs. As a further benefit, our use of anomalies reduces greatly the need to composite the meteorological data for days on which contrail outbreaks are absent: in a given month and location, these usually number considerably more than the days on which outbreaks occur—even in regions of relatively high frequency of outbreaks—and therefore would resemble the climatological normal (section 4a).

We infer the dominant physical processes attending contrail outbreaks occurring in otherwise clear or partly cloudy skies from the regional composites and within the context of results from previous case studies. Where relevant, we compare the synoptic climatology with the all-U.S. "climate diagnostics" (CDNs) of outbreaks determined for early–mid-September periods of 1995–2001 (Travis et al. 2004). These CDNs comprise statistical "models" of outbreaks developed by averaging meteorological anomaly fields on a moveable grid (cf. Martin and Salomonson 1970; Businger et al. 1990). Although the CDN statistics are not specific to a given region or subregion, they permit the associated dominant dynamic and thermodynamic atmospheric structures to be inferred [cf. the rawinsonde-derived temperature profiles of contrail outbreak cases presented in DeGrand et al. (2000)]. In particular, we consider the spatial associations of contrail outbreaks with nearby thick natural clouds, including cirrus, by comparing their respective CDNs.

2. Regionalization of contrail outbreaks

The synoptic climatology of contrail outbreak atmospheric environments derived here requires a regionalization of the conterminous United States, which we develop based upon the geographical areas of high contrail frequency identified in previous satellite-based spatial climatologies (DeGrand et al. 2000; Palikonda et al. 2005; Travis et al. 2007). These show persisting contrail frequency maxima in the following nominal regions: the Midwest, the Northeast, the Southeast, the Southwest and Pacific Coast, and the Northwest; with minima in the Upper Great Plains and Intermountain West. Incorporating the contemporary period climatology of contrails (i.e., midseason months of 2000–02; Travis et al. 2007), our final regionalization (Fig. 2) comprises 10 regions that have much in common with the 9 regions used in Sun and Groisman's (2004, their Fig. 1) study of trends and changes in low-level cloudiness. Although the edges of each region (Fig. 2) mostly follow state boundaries, this is done largely to facilitate presentation; the boundaries are flexible and should be considered zones of transition. In assigning a satellite-observed contrail outbreak to a particular region, the outbreak was mostly or entirely located therein. Outbreaks that overlapped regions were assigned to the adjacent upstream (usually western) region, given the typical patterns of advection over middle latitudes.

3. Data and their analysis

a. NOAA AVHRR–based identification and GIS analysis of contrail outbreaks

We use the 1.1 × 1.1 km^2 resolution AVHRR IR data acquired by the *NOAA-12*, *-14*, and *-15* polar-orbiter platforms, for midseason months of 2000–02 (the synoptic climatology), and the early–mid-September periods of 1995–2001 (the CDNs). [These images (e.g., Fig. 1) are available free online from the U.S. National Climatic Data Center (NCDC) at http://www.class.noaa.gov.] In the 2000–02 period, a total of 2126 images, or median of 6 images per day, were examined for contrails and outbreaks over the entire United States. This frequency corresponds approximately to one image each for night, morning, and af-

ternoon in the eastern and also western halves of the country. For the early–mid-September periods (CDNs), 623 AVHRR images (an average of 10 images day^{-1}) were analyzed for outbreaks within the conterminous United States.

An outbreak occurring in otherwise clear or partly cloudy skies appears on the IR imagery as a lattice of intersecting contrails (Fig. 1). Accordingly, the manual interpretation (i.e., pattern recognition) method of identifying outbreaks developed by Carleton and Lamb (1986), and subsequently used to generate the contrail spatial climatologies of DeGrand et al. (2000) and Travis et al. (2007), readily is applied (e.g., Duda et al. 2001). An outbreak was determined to occur when the sky coverage showed at least one-quarter contrails; when natural clouds were present (e.g., cirrus, stratus), this criterion was increased to at least one-half coverage by contrails. The pattern-recognition method contrasts with more computer-intensive methods required to find line contrails embedded in thick cirrus and cirrostratus (e.g., Lee 1989; Mannstein et al. 1999; Meyer et al. 2002; Duda et al. 2005; Palikonda et al. 2005), and which rely on combinations of the IR temperature and the "split window" temperature difference. Given our emphasis on outbreaks occurring in otherwise clear air or only partly cloudy skies, we do not use the computer-based method here.

We applied GIS to determine the areal coverage, or size, of each outbreak (km^2) that includes both cloudy (from contrails and any natural clouds) and clear pixels, for the image time [t(max)] showing densest contrail coverage or maximum number of contrails. An outbreak was tracked over several images but only counted once, with the majority of outbreaks lasting at least 4–6 h (Travis and Carleton 2005). Determination of outbreak size involved drawing a "bounding box" aligned by latitude–longitude coordinates that encloses all the contrails within a given outbreak. Mean and variance statistics on outbreak size were stratified by region, midseason month, and year, and then combined for further analysis at regional and seasonal levels. In determining the CDNs of thick clouds, including cirrus, for comparison to those of contrail outbreaks, comparable-sized areas were selected from thick high and cold clouds that often were located upstream of outbreaks but in the same general region. Contrails may have been present within some of these natural cloud areas (cf. Mannstein et al. 1999).

b. NCEP–NCAR reanalysis (NNR) data

The synoptic climatology uses NNR data of assimilation model-analyzed fields (Kalnay et al. 1996; Kistler et al. 2001); more specifically, mapped daily averages of the four 6-hourly (0000, 0600, 1200, and 1800 UTC) analyses and their departures from the long-term daily means. The CDNs compiled separately for contrail outbreaks and samples of thick clouds, rely upon NNR data at the 6-h time nearest the satellite overpass corresponding to t(max). (Both NNR datasets are available online at http://www.cdc.noaa.gov/.) Because the NNR are "global reanalyses" with a nominal grid resolution of 2.5° × 2.5°, they are appropriate for determining the synoptic-scale atmospheric environments associated with contrail outbreaks. Moreover, the different temporal resolutions of the data used (daily-averaged, 6-h) permit intercomparisons between the two sets of composites that are derived.

In selecting NNR variables to be composited (Table 1: 14 variables for a total of 37 levels or layers, including the tropopause), we were guided by previous research on contrail–meteorological condition associations at synoptic and smaller scales (refer to the introduction), most notably the following studies: Appleman (1953), Pilié and Jiusto (1958), Schumann (1996), Travis

TABLE 1. Meteorological variables and derived quantities acquired from NNR daily-averaged (4 per day) and 6-h maps, used in the composite analysis of contrail outbreak environments. Reliability classes are according to Kalnay et al. (1996, their appendix A). Reanalysis A variables are strongly influenced by observations; B variables are influenced both by observations and the model.

Variable	Level(s), hPa	Units	Reliability class
Geopotential (Z)	500, 300, 250, 200	m	A
Pressure (p)	sea level, (tropopause)[a]	hPa	A
Air temperature (T)	300, 250, 200, (tropopause)[a]	°C, K[b]	A
Vector wind ($\mathbf{V}$)	500, 300, 250, 200	m s^{-1}	A
Zonal wind (u)	500, 300, 250, 200	m s^{-1}	A
Meridional wind (v)	700	m s^{-1}	A
RH	500, 300	%	B
SH	500, 300	g kg^{-1}	B
Omega (ω), $=dp/dt$	500, 300, 250, 200	hPa s^{-1}	B
[c]Thickness (dZ)	300 – 200, 300 – 250	m	—
[c]Lapse rate (dT)	200 – 300, 250 – 300, 200 – 250	K[b]	—
[c]u vertical shear (du)	200 – 300, 200 – 250	m s^{-1}	—
[c]$\mathbf{V}$ vertical shear ($d\mathbf{V}$)	300 – 200	m s^{-1}	—
[c]Layer-avg ω	300–250, 300–200	hPa s^{-1}	—

[a] Available for online monthly-averaged NNR data.
[b] Air temperature is in degrees Celsius for online NNR daily-averaged, monthly-averaged, and long-term means and in kelvins for 6-h NNR data.
[c] Derived quantities.

(1996a), Schrader (1997), Travis et al. (1997), Kästner et al. (1999), and Duda et al. (2004). Thus, we use the tropopause-level (when available, Table 1) and UT data on temperature and pressure/height. Wind parameters (e.g., speed, directional shear) at aircraft flight level are important for contrail spreading, and thus are of some importance for persistence (e.g., Newton et al. 1997; Travis 1996b; Jensen et al. 1998). Further, their values in the UT should exhibit close associations with synoptic circulation. Accordingly, we use the UT standard-level data on vector winds (**V**) and the u-wind component, as well as the vertical shear (i.e., difference between **V** at 300 and 200 hPa). The vertical motion is given as omega (ω) = dp/dt, whereby negative values indicate ascent of air and positive values subsidence. Moreover, the spatial variation of omega at least partly explains the anomalies of free-atmosphere moisture: we use both specific humidity (SH) and relative humidity (RH; Table 1), as justified from the analysis of spatial and temporal coherence among atmospheric moisture variables conducted by Dee and Da Silva (2003). However, a limitation of the NNR humidity data is their availability only up to 300 hPa, which is below the pressure altitude at which many jet aircraft generate contrails (Grassl 1990). This lack of information on moisture at higher altitudes reflects the unreliability of UTH measurements (e.g., Ross and Elliott 2001; Minnis et al. 2003, 2004), and is a common problem for research on contrails (e.g., Peters 1993; Chlond 1998; Poellot et al. 1999; DeGrand et al. 2000; Miloshevich et al. 2001; Duda et al. 2004). Accordingly, the composites of SH(300) and RH(300) that we derive should be considered a guide to humidity conditions in the UT—from the locations of anomaly centers of maxima and minima, and synoptic spatial gradients—rather than depicting actual values of moisture at flight altitudes. Last, to help to infer the pattern of thermal advection in lower- to midtroposphere (e.g., for comparison to maps of tropospheric thickness or temperature seen in Table 1), we composite the meridional (v) component of the total wind at 700 hPa [v(700)]. This is given as negative for northerly flow, and positive for southerly flow.

For the CDNs of contrail outbreaks and also dense clouds, including cirrus (i.e., September period), we compute the following additional variables from NNR mapped fields (Table 1) that are proxies for UT static stability and inferred baroclinity on synoptic scales (cf. Chlond 1998): the thickness [=Z(lower) − Z(upper)] for two layers; temperature lapse rates, determined from the vertical differences of temperature at three standard levels; the u vertical shear [=u(upper) − u(lower)] determined for two layers; and the vertically averaged omega for two layers (e.g., Reichler et al. 2003).

TABLE 2. Contrail outbreak frequencies and mean sizes of outbreak areas for the conterminous United States and adjacent areas (i.e., all subregions), midseason months of 2000–02. Chi-square (χ^2) statistic for outbreak frequencies = 29.06 ($p < 0.001$; critical value = 22.46 with 6 degrees of freedom), indicating that the cell frequencies are highly significantly different from an expected distribution calculated from the row and column totals, and the grand total (267).

Year	January	April	July	October	Total
2000	10	33	10	22	75
2001	28	22	14	37	101
2002	20	30	28	13	91
Total	58	85	52	72	267
Mean size ($\times 10^5$ km^2)	2.57	3.14	3.40	1.95	2.83
Std dev of size ($\times 10^5$ km^2)	2.42	2.82	2.80	1.62	2.59

With the notable exception of moisture (SH, RH), most NNR variables were acquired for the 500-, 300-, 250-, and 200-hPa standard levels (Table 1; cf. Ponater et al. 2002). Although intercorrelations among certain variables and adjacent levels (e.g., SH and RH at 300 hPa; omega at 300 and 250 hPa) introduce some redundancy, we include these as a mutual check on the results. Moreover, a synoptic analyst interested in predicting CFAs may not have data on all relevant variables for a given time.

In deriving the CDNs of contrail outbreaks versus thick and/or multilayered clouds, we linearly interpolated the NNR values between adjacent 6-h maps when the time difference (image minus NNR) exceeded ±2 h. To accommodate the large size range of outbreak GIS bounding boxes (section 4b), and to make intercomparable the outbreak-associated meteorological conditions for different regions, we expressed all NNR map values as departures from the 30-yr 9-day means (i.e., 1971–2000; 8–16 September) for that variable, level, and geographic location. We derived spatially weighted (by bounding box area) means and standard deviations of meteorological variables.

4. Results and discussion

a. Interseasonal and regional variations of contrail outbreaks, 2000–02

Averaged over the three years, contrail outbreaks occurring in clear or partly cloudy skies for the conterminous United States and adjacent areas (Table 2) exhibit a maximum frequency in the transition midseason months (i.e., April, October) and a minimum in July, with January having frequencies between these extremes. Similar results were shown for all contrails (i.e., those occurring both singly and composing outbreaks)

TABLE 3. Satellite-retrieved (AVHRR) frequencies and synoptic (NNR) attributes of contrail outbreaks for the 8–16 (early–mid) September periods of 1995–2001.

Variable	1995	1996	1997	1998	1999	2000	2001	All
Frequency	6	14	11	12	2	9	5	59
Normal[a]	13.6	18.7	17.7	16.4	1.7	9.2	4.3	9.5
Ridge[b]	5	7	5	8	1	9	4	39
Trough[c]	1	7	6	4	1	0	1	20

[a] Outbreak frequency normalized to every 100 images.
[b] Frequency (nonnormalized) of outbreaks associated with anticyclonic flow implied by the height contours at 300 hPa (e.g., Newton et al. 1997).
[c] Frequency (nonnormalized) of outbreaks associated with cyclonic flow implied by the height contours at 300 hPa.

in midseason months of 1977–79 (DeGrand et al. 2000), suggesting a climatic first-order association with the atmospheric westerly circulation and jet stream: on average, the circumpolar vortex and jet stream expand and are displaced furthest south—over U.S. southern states—in winter, and contract northward—over southern Canada—in summer, and occupy intermediate latitudes in the transition seasons. The contrail outbreak minimum in July (Table 2) likely reflects reduced baroclinic activity over most of the conterminous United States at that time (DeGrand et al. 2000), and a predominance of convectively derived cirrus (e.g., Jasperson et al. 1985). An association of the latter feature with contrails was noted by Palikonda et al. (2005) to be especially pronounced in the afternoon hours.

The frequency variations of contrail outbreaks are highly significantly different ($p < 0.001$ level) across midseason months (i.e., column values) and years (rows). Because aircraft flight frequencies show little variation when averaged temporally (e.g., monthly) (BACK Aviation Solutions 2005; Travis et al. 2007), these significant differences imply an outbreak dominant association with atmospheric circulation variations (DeGrand et al. 2000), although spatial associations between temporally averaged aircraft flight density and contrail outbreak frequencies are evident (section 4b, below). Of the three years analyzed, the greatest incidence of outbreaks occurred in 2001 (101); the least occurred in 2000 (75). The substantial interannual departures from the midseason average outbreak frequencies include those of 2002, when higher frequencies occurred in April and July and the lowest occurred in October. Large interannual variations in outbreak frequencies also occurred for the seven submonthly periods each composed of 9 days in early–mid-September of 1995–2001 (Table 3). Again, these results imply the importance of UT (here represented by the 300-hPa level) meteorological conditions for the persisting contrails composing outbreaks (Travis and Carleton 2005), examined in section 4c.

Stratifying the 2000–02 midseason outbreak frequencies by United States regions (Table 4) reveals strong areal differentiation, as also was evident in previous studies that combined single and multiple (i.e., outbreak associated) contrails (DeGrand et al. 2000; Minnis et al. 2003; Palikonda et al. 2005). The Midwest experienced by far the greatest number of outbreaks (32.6% of U.S. total), followed by the Northeast (17.6%) and Southeast (17.2%). The outbreak maximum frequencies in the Midwest result from this region's location beneath the major transcontinental flight corridor linking the large cities of the U.S. East and West Coasts, with its high density of UT flights (Changnon 1981; Palikonda et al. 2002, their Fig. 3), along with the frequent occurrence of highly favorable meteorological conditions [section 4d(1)]. Regions of the western and southwestern United States had some of the lowest outbreak frequencies in the study years. Although the regional pattern of high outbreak frequencies (Midwest, Northeast, Southeast) for 2000–02 is broadly similar to that shown for all contrails during

TABLE 4. Contrail outbreak frequencies in descending order for the 10 subregions composing the conterminous United States (refer to Fig. 2), and mean sizes of outbreak areas; 3-yr midseason months (2000–02).

Region	Area $\times 10^5$ km^2	January	April	July	October	Total	Mean size $\times 10^5$ km^2	CCF, %*
Midwest	10.94	15	29	20	23	87	3.75	8.1
Northeast	6.81	8	14	15	10	47	3.71	6.9
Southeast	5.40	15	13	8	10	46	3.19	7.4
South	5.85	12	3	0	11	26	3.03	3.7
Great Plains	11.22	2	5	1	6	14	3.70	1.3
Northwest	4.26	1	8	2	2	13	1.93	1.6
West Coast	4.09	0	5	4	2	11	2.92	2.1
Great Basin	9.59	1	5	1	3	10	2.80	0.8
Southwest	8.43	4	1	1	3	9	1.07	0.3
Intermountain	11.20	0	2	0	2	4	3.70	0.4

* CCF = (total $\times$ mean size)/(area $\times$ observations).

the midseason months of 1977–79 (DeGrand et al. 2000), this departs significantly for the West and Southwest. The relative lack of outbreaks over and near California in the contemporary period may reflect the interdecadal change in large-scale UT meteorological conditions noted by Travis et al. (2007), whereby the tropopause in the western United States lowered and warmed, on average, between the mid-to-late 1970s and early 2000s, while it rose and cooled in the eastern United States. We have attributed at least part of this change in the tropopause to a temporal trend in the Arctic Oscillation (Travis et al. 2007). An additional possibility is that outbreaks may be less common than individual contrails near the West Coast, where fewer flights connect the United States with international destinations, contrasted with the number of domestic flights. In this regard, Minnis et al. (2005) identify individual long and persisting contrails near and off the coast of northern California for 4 months in 2002 and 2003.

The information on contrail-outbreak regional frequencies (Table 4) shows no obvious association with climatological cloud amounts: regions of the United States having some of the greatest cloud amount values (e.g., the Northeast) have high frequencies of outbreaks, while others having climatologically low frequencies of cloud amount (the Southwest and intermountain) have minimal outbreak occurrences. This both supports the pattern-recognition method of finding contrail outbreaks in clear or partly cloudy skies, and helps ensure that the regional synoptic atmospheric composites we derive are representative of contrail outbreak environments distinct from those of dense natural cloudiness (e.g., those associated with frontal systems).

b. Satellite-retrieved size of contrail outbreaks

The GIS-derived mean size of contrail outbreaks in the 2000–02 midseason months is close to 3×10^5 km^2 (Table 2), confirming their synoptic-scale atmospheric association (cf. Barry 1970), although with large variability about the mean. Comparing the contrail-outbreak total coverage with the total number of days analyzed (369) yields a mean outbreak coverage for the conterminous United States of 2.29×10^5 km^2 day^{-1}, which corresponds to approximately 5% of the land area within the conterminous United States, or an area slightly less than the state of Montana (Travis and Carleton 2005). Similar to the frequencies of contrail outbreaks (Table 2), there are substantial interseasonal differences in outbreak mean size, being largest in July and smallest in October. Interestingly, the former occurs in the midseason month having the average minimum frequency of outbreaks, while the latter can occur in the midseason month of maximum frequency. The mean size of outbreaks we derive is considerably larger than some of the contrail "cluster" cases studied by Duda et al. (2001, 2004), and likely results from differences in defining groups of contrails in the two sets of studies: Duda et al. compute contrail coverage using a bispectral threshold method that includes only cloudy (because of contrails) pixels; our GIS-based method includes both cloud-covered (contrails and any natural clouds) and intervening clear-sky pixels within the outbreak. For estimating the radiative impact of contrail outbreaks, the Duda et al. method is preferred; for identifying the synoptic atmospheric circulation associations of contrail outbreaks, the GIS-derived size of the entire outbreak is appropriate.

There are also substantial regional differences in the typical normalized (by regional area) size of contrail outbreaks occurring in clear or partly cloudy skies (Table 4). Although the regions of highest frequency (i.e., the Midwest and Northeast) have the largest mean sizes of outbreaks, two regions of relatively low frequency (Great Plains, Intermountain) also see larger-sized outbreaks. This finding likely indicates the role of flight densities (i.e., frequencies and spatial concentrations), where these are greater in the Midwest and eastern United States, on average, yet reduced and more dispersed in the West (Palikonda et al. 2002, their Fig. 3). Potentially significant to the synoptic climatology of outbreaks is that the Northwest sees one of the smallest mean values of outbreak normalized size (1.93×10^5 km^2): outbreaks in this region typically are associated with different synoptic circulation conditions than those characterizing the eastern United States [section 4d(4)].

To better permit interregional comparisons of the statistics on contrail-outbreak frequency and size, we incorporate both variables into a "contrail coverage" factor (CCF; Table 4, last column). Thus, a location in the Midwest has around an 8% probability of being covered by a contrail outbreak, while the Northeast and Southeast regions have close to a 7% probability. In contrast, U.S. regions west of the Mississippi River—with the exception of the West Coast (i.e., California)—have CCF probabilities $<2\%$, especially in interior locations (Great Basin, Southwest, Intermountain). These results imply an additional 2% cirrus cloud coverage for U.S. regions having high frequencies of contrail outbreaks (the Midwest, Northeast, Southeast), given our satellite image-based criterion of one-quarter sky coverage due to contrails (section 3a).

c. Outbreak associations with monthly-averaged regional atmospheric circulation

Figure 3 shows the regional dependence of the marked interannual variations (2000–02) of contrail

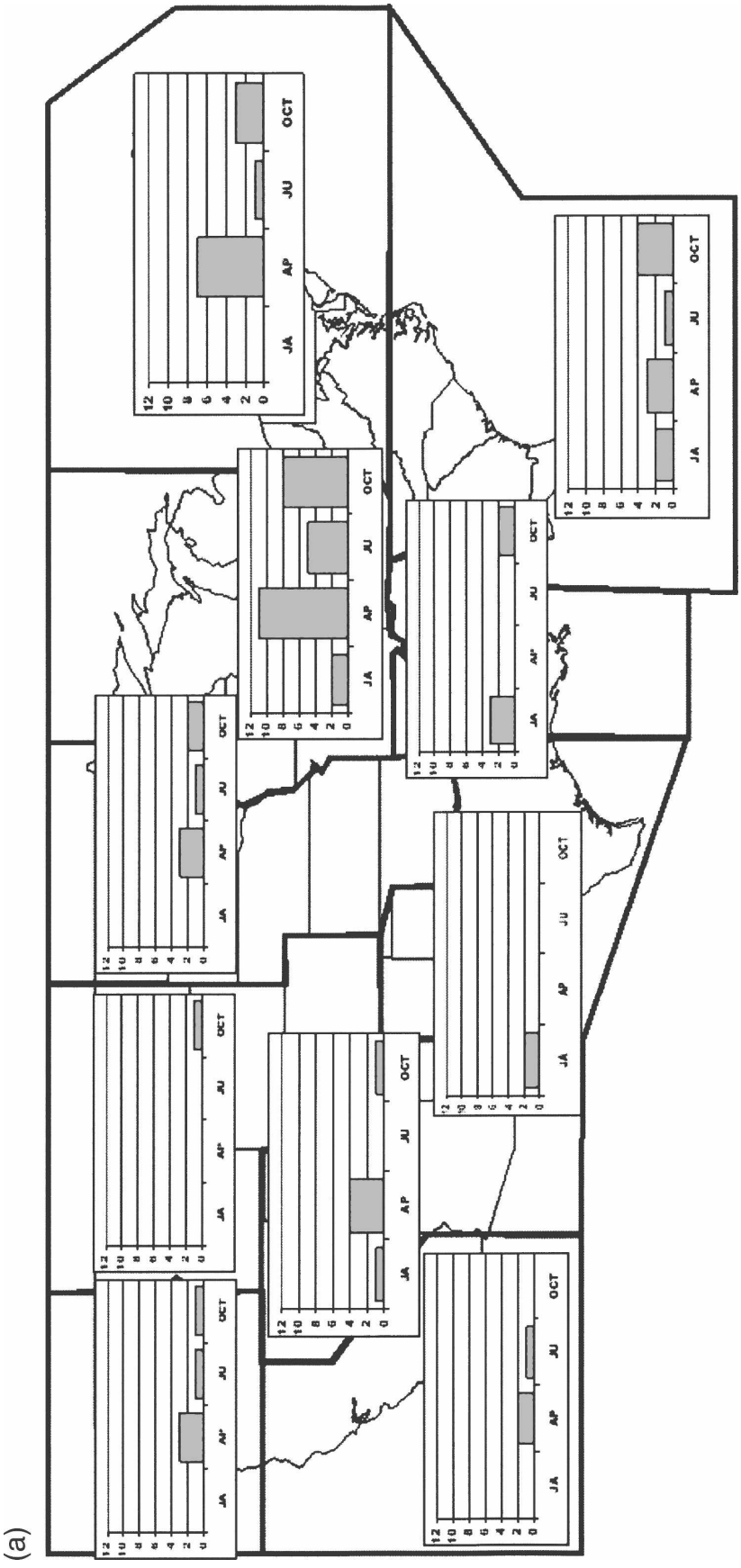

FIG. 3. Annual midseason month totals of contrail outbreaks by U.S. region (Fig. 2), determined from interpretation of AVHRR images for (a) 2000, (b) 2001, and (c) 2002. The labels on the horizontal axis identify the month, as follows: Ja = January, Ap = April, Ju = July, and Oct = October.

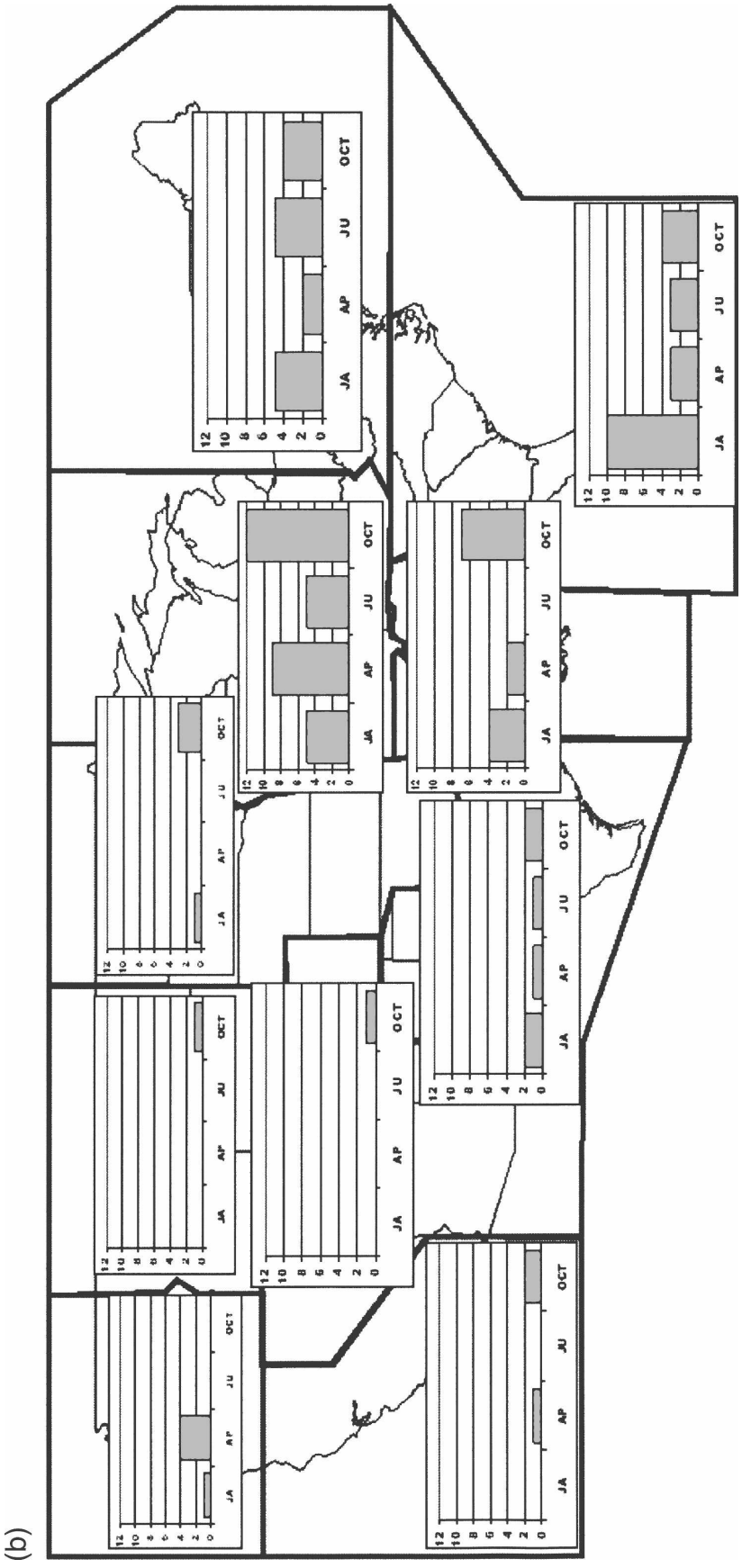

FIG. 3. (*Continued*)

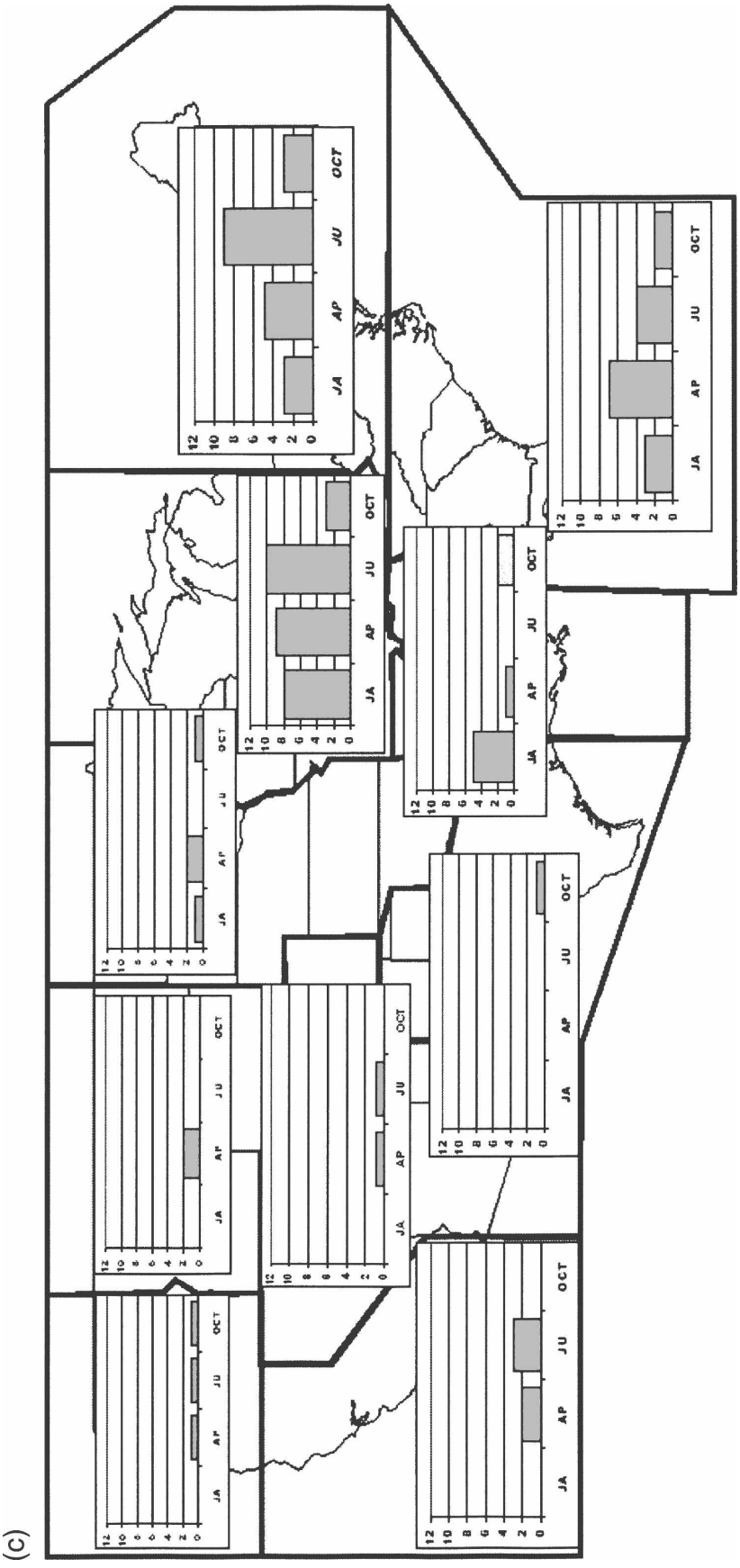

FIG. 3. (*Continued*)

outbreaks. Prior to deriving the regional synoptic climatologies of contrail outbreaks, we investigated the possibility that midseason monthly-averaged atmospheric circulation differences between extreme years might show broad associations with the interannual variations of outbreak frequencies (cf. DeGrand et al. 2000, their Figs. 8–10). To better match the spatial scale of the monthly-averaged circulation, we analyzed those midseason months having large year-to-year variations in outbreak frequencies that were in the same direction (i.e., either many or few) for at least two adjoining regions. Given also the CCF results (Table 4), we were particularly interested in contrail outbreak large variations for regions east of the Mississippi River. Thus, obvious examples to examine were the Midwest, Northeast, and Southeast in July 2002 (maximum frequencies) and July 2000 (minimum frequencies; Figs. 3c,a), and the October months of 2001 and 2002 (Figs. 3b,c). The latter had, respectively, maximum and minimum frequencies for the Midwest, the Great Plains, and the South. We used the NNR monthly-averaged anomalies for a number of UT variables (Table 1), and subtracted the variable means for the month of outbreak lowest frequencies from the month of highest frequencies.

The July differences (i.e., 2002 minus 2000, Fig. 4) are consistent with previous results documenting the association between UT conditions and persisting contrails (e.g., Appleman 1953; Pilié and Jiusto 1958; Schrader 1997; Jensen et al. 1998; DeGrand et al. 2000), and also with the results for individual U.S. regions when composited only for the days on which contrail outbreaks occurred (section 4d). In July 2002, the greater frequencies of contrail outbreaks over the Midwest, Northeast, and Southeast had associated monthly-averaged atmospheric difference patterns for the larger region, as follows: higher geopotential heights accompanying tropospheric ridging (Fig. 4a); greater thickness (Fig. 4b) resulting from a warmer troposphere; spatial gradients of omega that represent increasing ascent of air in the UT on moving westward (Fig. 4c); similarly enhanced spatial gradients of humidity, at least up to around 300 hPa (Fig. 4d); and weaker zonal westerlies in the UT but with tight gradients implying horizontal shear northward (Fig. 4e). There is reduced pressure and lower temperature at the tropopause level, particularly over the more northern parts of the study region (Figs. 4f,g); around the cruise altitudes typical of jet aircraft on medium- and long-haul flights (e.g., Grassl 1990, his Fig. 1). For aircraft flying above the tropopause (e.g., over more northern latitudes and/or in the cold season), the lower humidity of the stratosphere precludes persistent contrails. That the tropopause-level anomalies do not extend over the southeastern United States (Figs. 4f,g) probably results from the fact that most contrail outbreaks occurred in the Midwest and Northeast subregions in July 2002 (Figs. 3a,c), and thus may speak to the problem of deriving spatial composites for too large a region. Despite the temporal smoothing of the monthly-averaged data, these results generally support a previously suggested (e.g., DeGrand et al. 2000) atmospheric regime accompanying persisting contrails and outbreaks of positive height anomalies and a warmer troposphere with, consequently, a higher and colder tropopause.

The CDN results for early–mid-September (1995–2001) generally are consistent (Table 3) with the synoptic associations of contrail outbreaks determined for the July months of 2000 and 2002 (Fig. 4). They support previous aircraft-level and satellite-based findings of increased contrail occurrence in two broad locations within the upper wave pattern: in areas of significant warm advection in the UT (i.e., near and west of ridges) and also cold advection (in and west of troughs; Changnon et al. 1980; Carleton and Lamb 1986; Kästner et al. 1999; DeGrand et al. 2000). Of the 59 outbreaks observed on the imagery, 39 occurred in or near UT height ridges, and 20 occurred in or near UT troughs, or a ratio approximately 2:1. Accordingly, area-weighted mean composites of NNR UT variables for the early–mid-September period (Travis et al. 2004) give a thickness [$Z(300 - 200)$] anomaly = −6.5 m, and a 300–200-hPa lapse rate of −1.6 K (i.e., colder air with an elevated tropopause); weak easterly wind anomalies [$u(300) = -2.5$ m s^{-1}]; and weak upward vertical motion [e.g., $\omega(250) = -5.4 \times 10^{-5}$ hPa s^{-1}]. Moreover, the spatial range of composite RH(300) across the contrail outbreak was greater than climatology from +7.5% to +58.0%.

For October (2001 − 2002), consistent associations between multiregion contrail-outbreak frequency variations and the monthly averages of atmospheric variables are less evident (not shown). Although UT winds were weaker in 2001 than in 2002, as they were also in the two July months of greater outbreak frequencies, most other variables show either opposite patterns (e.g., a lower and warmer tropopause in 2001, sinking air in UT) or patterns that change sign across the adjacent regions of the Midwest, the Great Plains, and the South (e.g., 1000–500-hPa thickness; UT temperature; SH and RH in mid–upper troposphere). This lack of consistency in outbreak-associated atmospheric conditions for the two October months studied likely results from the greater vigor and within-month variability of the atmospheric circulation at this time of year. These climatological features accompany strong latitudinal temperature gradients and, consequently,

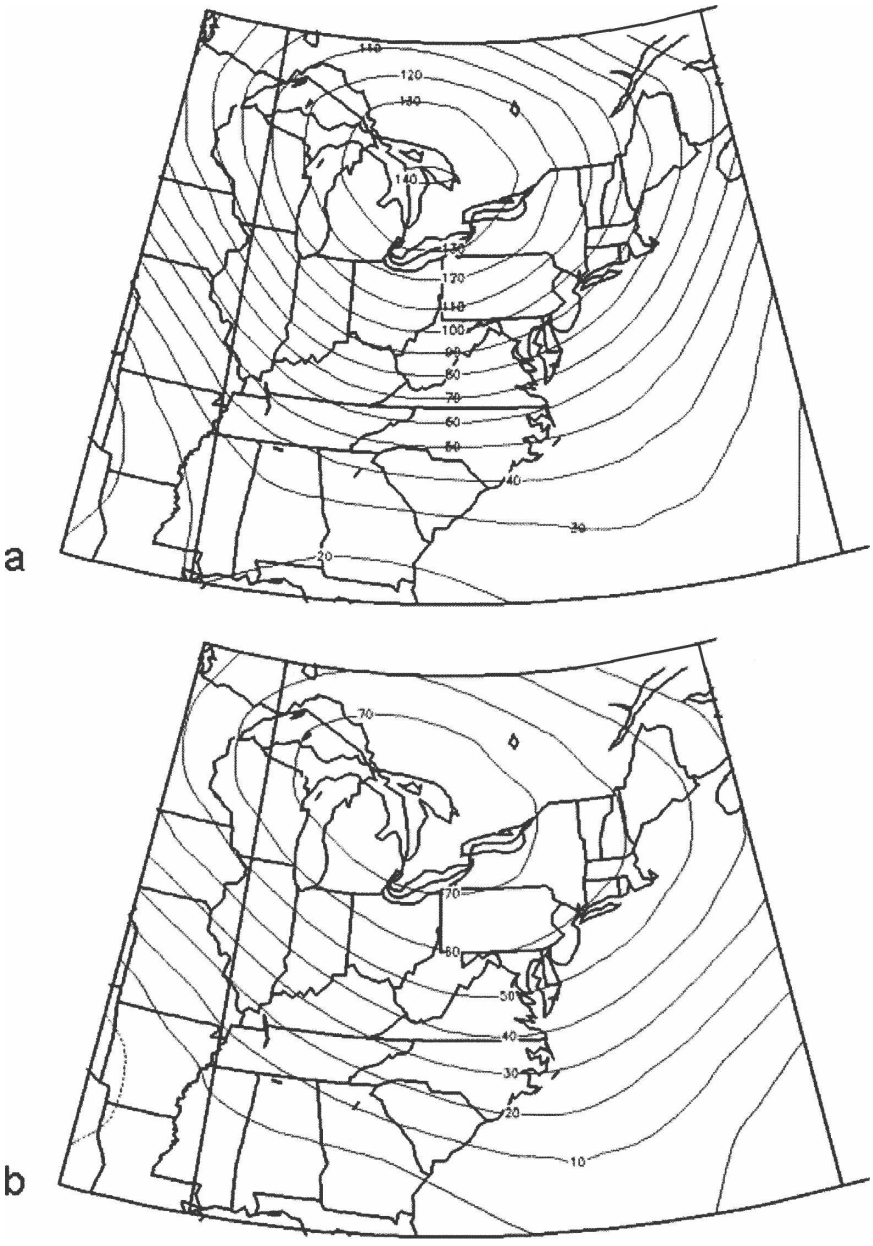

FIG. 4. Difference maps (July 2002 − 2000) of atmospheric variables for the Midwest, Northeast, and Southeast conjoint regions, based on monthly-averaged NNR data: (a) $Z(300)$, m; (b) $Z(1000 - 500)$, m; (c) $\omega(300)$, Pa s^{-1}; (d) RH(300), %; (e) $u(300)$, m s^{-1}; (f) tropopause pressure, hPa; (g) tropopause temperature, °C.

enhanced regional differences in circulation across latitude zones (cf. the Midwest, South). Because the use of monthly-averaged atmospheric fields masks the transient meteorological conditions associated with contrail outbreaks, especially during the transition seasons, elucidation of their synoptic atmospheric associations requires that the NNR daily data be composited for days on which outbreaks occurred in a given region (below).

d. Synoptic climatology of contrail-outbreak atmospheric conditions, 2000–02

The synoptic climatology of contrail outbreak-associated atmospheric anomalies is presented for U.S. subregions having higher frequencies of outbreaks and CCF values for the 2000–02 midseason months; the Midwest, Northeast, and Southeast (Table 4). In addition, we show results for the Northwest (sixth in terms

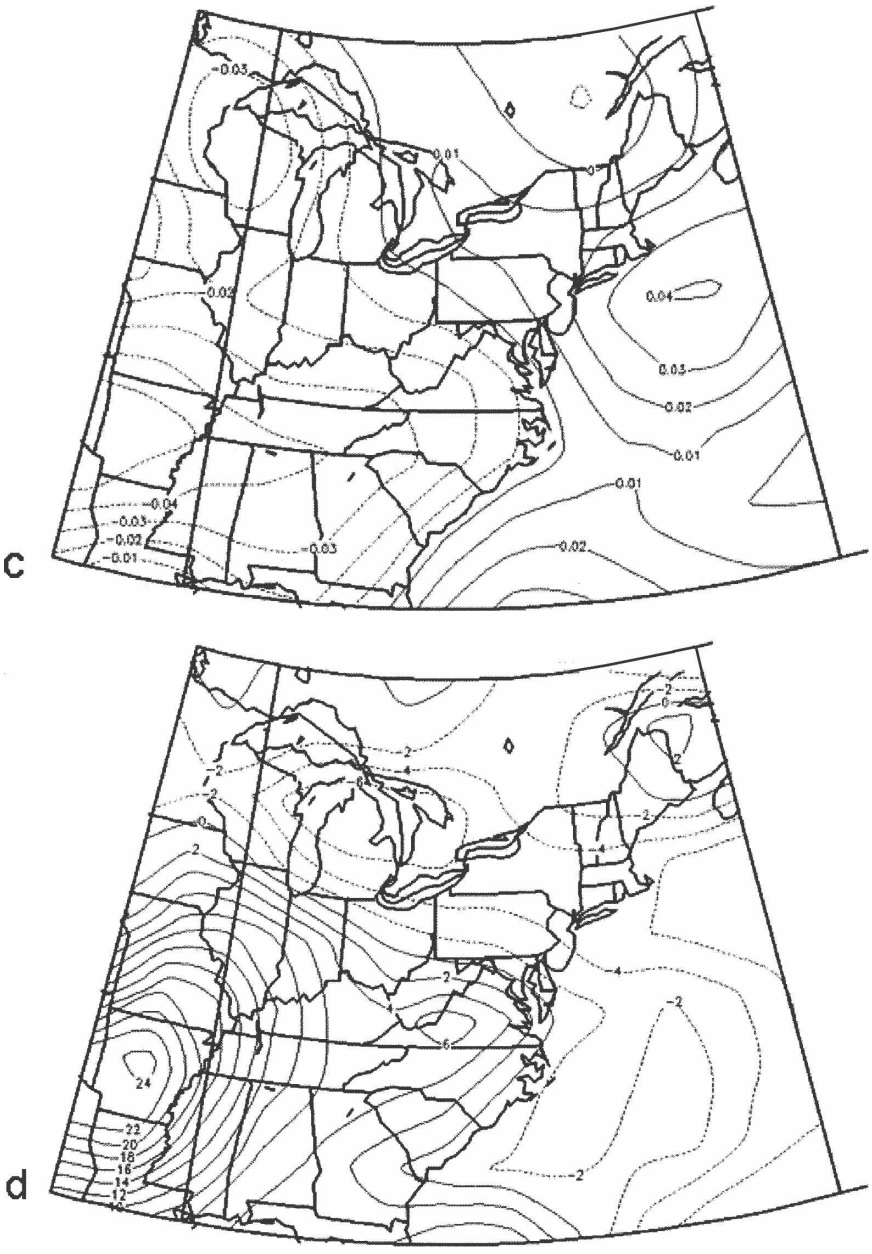

FIG. 4. (*Continued*)

of outbreak frequencies) because the synoptic climatology for this region differs from that accompanying outbreaks in other regions; that is, there is evidence of geographic variation in contrail outbreak synoptic environments. Given the large seasonal variation in tropopause height, especially over more northern regions of the conterminous United States (e.g., Fig. 4f), we show the all-season composite UT maps only for the 300-hPa surface: meteorological data on pressure surfaces at higher altitudes (e.g., 250 hPa: Table 1) will include the stratosphere, especially in the colder season. Moreover, the 300-hPa height, wind, and vertical motion fields are more readily compared with those of moisture (RH, SH), which are only available up to 300 hPa. Regional atmospheric composites stratified by midseason month (not shown) are similar to the all-months composites presented in Figs. 5–8, but with an intensification of the anomaly gradients generally being evident in January and April, and a relaxation in July and October. This seasonal variation also was shown in the DeGrand et al. (2000) spatial climatology of all contrails.

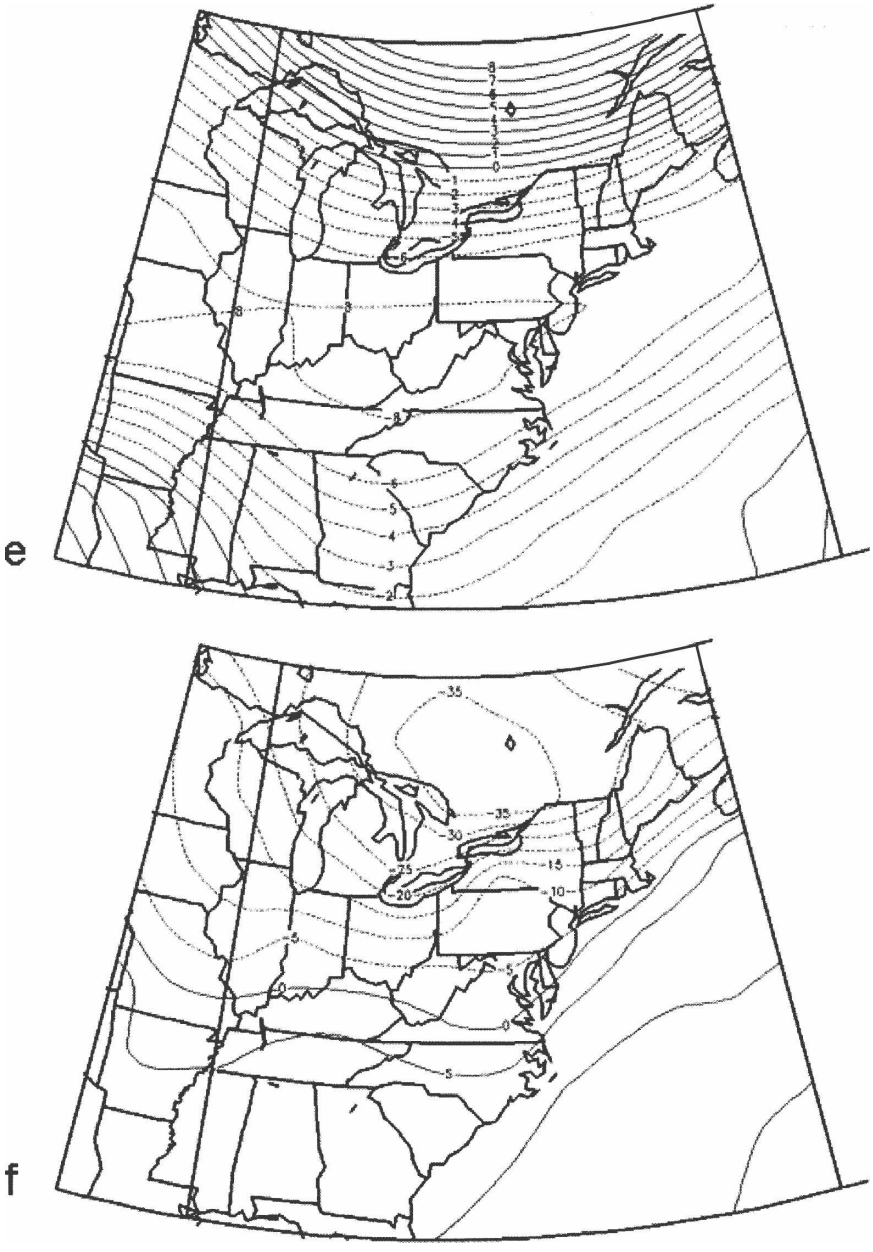

FIG. 4. (*Continued*)

1) THE MIDWEST

For the Midwest, contrail outbreaks typically are associated with strong positive anomalies of tropospheric pressure/height (i.e., enhanced geopotential ridge) that slope westward with altitude (Fig. 5a). Consistent with these pressure/height anomalies are the composite lower–midtroposphere vector winds (not shown) and meridional component of the wind (Fig. 5b): the latter changes from negative (i.e., northerly) in eastern areas to positive (i.e., southerly) in western areas, in advance of an approaching trough. The warm-cored ridge is confirmed by the composite temperature anomaly fields for different standard levels within the troposphere (e.g., at 500 hPa: Fig. 5b) and the 1000–500-hPa thickness (not shown), all of which indicate positive anomalies increasing toward western parts of the region. As shown in section 4c, this ridge pattern accompanies a tropopause that is both higher and colder than the long-term mean for the date. Composite anomalies of omega for the mid–upper troposphere (Fig. 5c) show Midwest contrail outbreaks to be associated with a north–south-oriented strong gradient of vertical motion, comprising positive anomalies (i.e., subsidence) to the east and

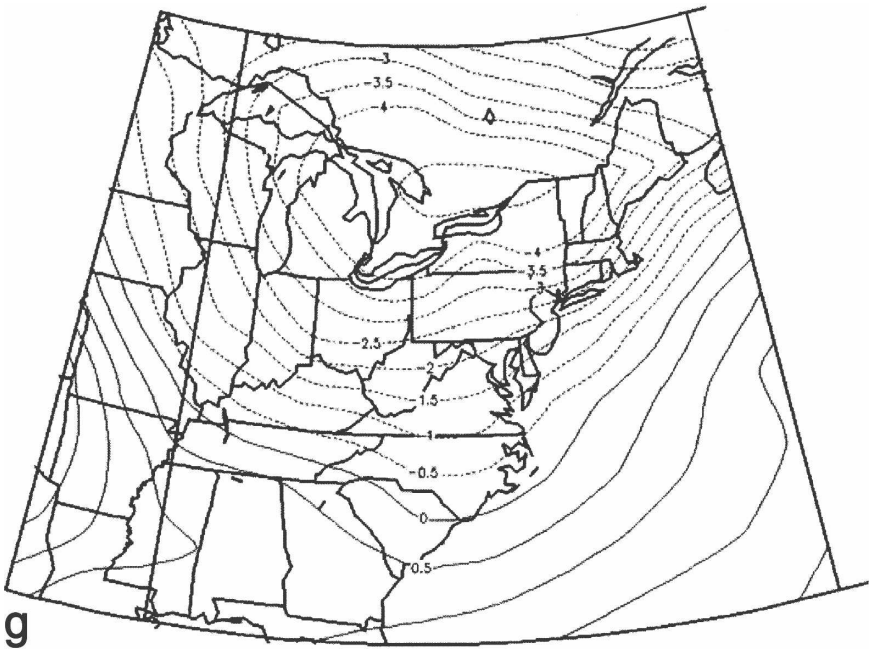

FIG. 4. (*Continued*)

negative anomalies (ascent) to the west. Thus, outbreaks in clear or partly cloudy skies occur, on average, when and where UT air motions change from weakly subsiding to weakly rising; between a ridge located to the east, and a trough to the west. Accordingly, moisture anomalies in the mid to UT (Fig. 5c) are strongly negative (i.e., dry air) to the southeast, and become weakly negative to slightly positive (moister air) in the north. These patterns also are consistent with the UT zonal winds (Fig. 5d), whereby negative (i.e., reduced westerly) and positive (i.e., stronger westerly) anomalies are located to the southeast and northwest, respectively, with a zone of relatively tight gradient oriented northeast–southwest through the Midwest. The *u*-wind anomaly pattern accompanying contrail outbreaks implies a jet maximum composite location in the northern Midwest and south-central Canada—associated with the upstream trough—having upward vertical motion and, hence, moistening of the air over the Midwest.

2) THE NORTHEAST

The synoptic climatology of contrail outbreaks for the Northeast region is broadly similar to that for the Midwest, but with additional features that seem to correspond, at least in part, to the effects of land–sea contrasts on synoptic systems. As in the Midwest, most outbreaks occur in association with positive anomalies of pressure/height through the troposphere (i.e., ridging; Fig. 6a). However, for the Northeast it is interesting that the surface high center associated with the upper ridge is located further northward, into southeast Canada, and shows ridging southward along the coast (Fig. 6a). Accordingly, this pattern has associated an anomaly axis of maximum negative $\upsilon(700)$ over the Northeast (Fig. 6b)—or northerly flow with implied cold advection—that decreases toward Ohio. In the free atmosphere below 300 hPa, anomalies of the 1000–500-hPa thickness (not shown) mostly are positive and increase toward the west, similar to the pattern of temperature anomalies in the middle troposphere and UT (Figs. 6b,d). This pattern of tight temperature gradients suggests a greater average baroclinity associated with contrail outbreaks in clear or partly cloudy skies than is evident for the Midwest region. Similarly, the gradient from omega positive anomalies (i.e., sinking air) along the coast to negative anomalies in the Great Lakes area in advance of the upstream trough is stronger than for Midwest outbreaks (Fig. 6c). Also consistent with the vertical motion pattern in the Northeast, the UTH anomalies are negative (i.e., dry air) over most of the region, but increase to the northwest and become positive north of the eastern Great Lakes (Fig. 6c). The zonal component of the UT wind is negative (i.e., reduced westerlies) over most of the region, but increases to the northwest to become stronger westerly in south-central Canada (Fig. 6d). As it did for the Midwest, this pattern implies a preferred location for contrail outbreaks on the southeastern fringe of a jet maximum that accompanies a mobile trough.

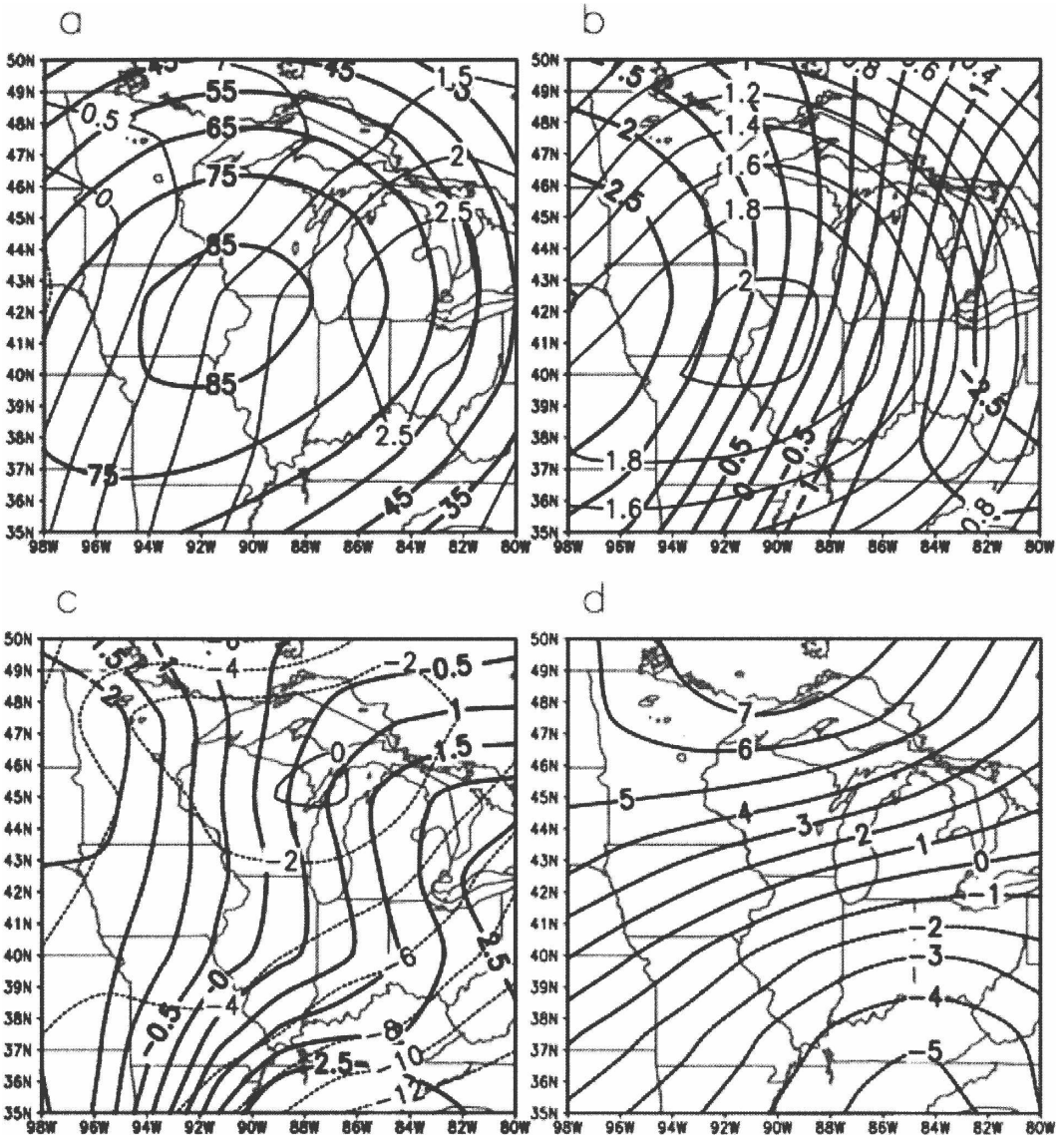

FIG. 5. The Midwest regional composite anomaly maps of daily-averaged NNR variables for contrail outbreaks in the midseason months of 2000–02 [number of days (n) = 68]: (a) $Z(300)$ and SLP (m: dark; hPa: light); (b) $v(700)$ and $T(500)$ (m s^{-1}: dark; °C: light); (c) $\omega(300)$ and RH(300) (hPa s^{-1} × 10^{-4}: dark; %: light); (d) $u(300)$ (m s^{-1}: dark). Full (dashed) lines in parts (a)–(d) denote positive (negative) anomalies. The difference in n composited from the total number of outbreaks for that region (Table 4) reflects the occurrence of days having more than one outbreak.

3) THE SOUTHEAST

The synoptic circulation composite patterns associated with contrail outbreaks in the Southeast are broadly similar to those in the Northeast and Midwest regions: positive height anomalies accompany ridging located to the northwest (Fig. 7a). In the lower–midtroposphere, a negative anomaly center in the meridional component of the wind field is located off the U.S. southeast coast, but this northerly component decreases on moving westward into Georgia and Alabama, in association with the circulation around the high pressure system (Fig. 7b). Accordingly, free-atmosphere temperature anomalies become increasingly positive to the northwest with gain of altitude, except at 300 hPa where negative anomalies occur above the coast (cf. Figs. 7b,d). Omega positive anomalies (i.e., sinking air) occur over most of the region, but with weakly negative anomalies (i.e., rising air) located over the interior Southeast. (Fig. 7c). Broadly consistent with this vertical motion pattern, RH anomalies in the UT (Fig. 7c) show gradients of UTH oriented south-

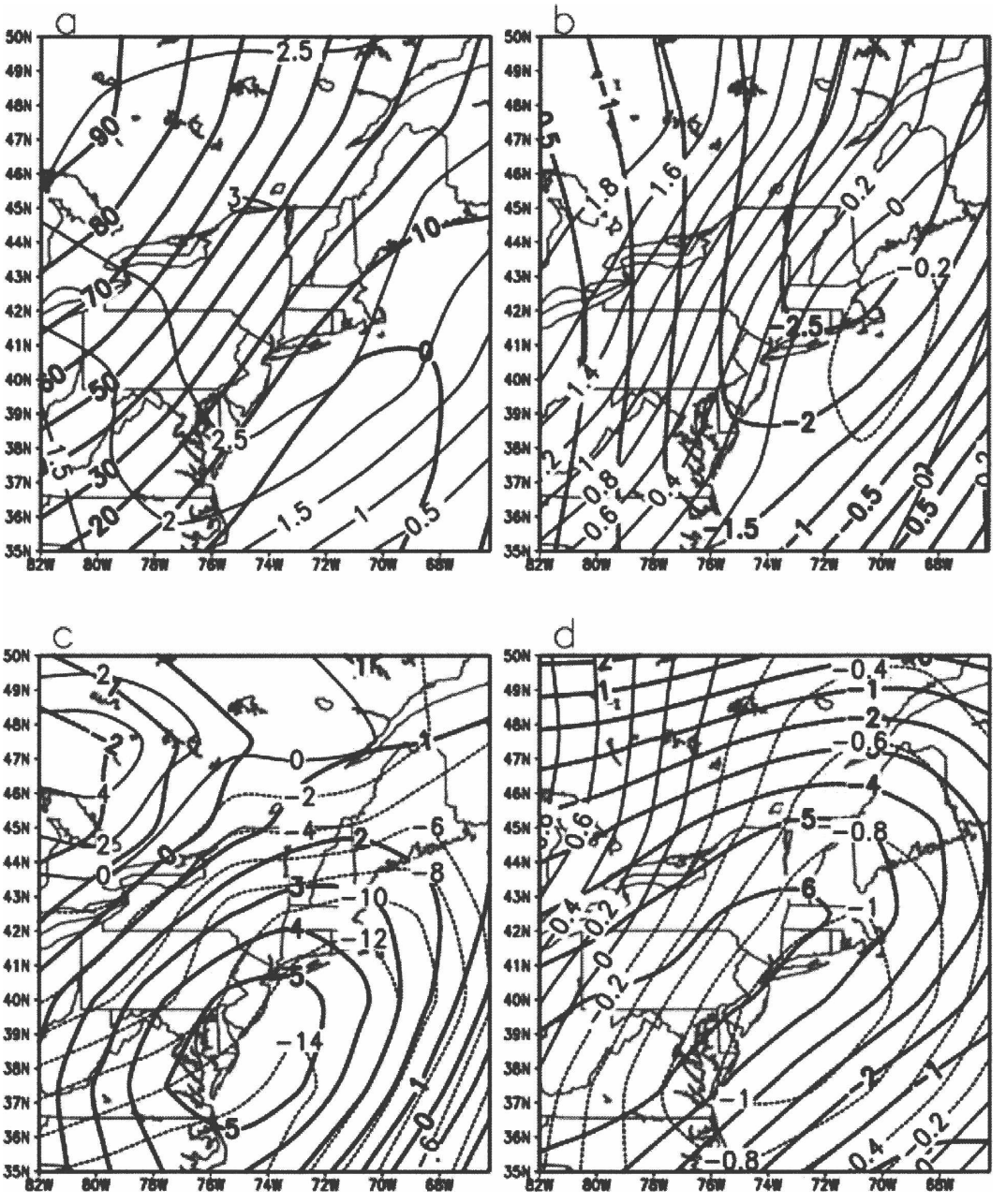

FIG. 6. Similar to Fig. 5, but for the Northeast (n = 42) and (d) u(300) and T(300) (m s^{-1}: dark; °C: light).

west–northeast, such that dry air is located to the southeast and moister air is over northwest parts of the Southeast. In contrast to the synoptic climatology of contrail outbreaks for the Northeast, that for the Southeast shows negative average anomalies of zonal wind over just about the entire region (Fig. 7d).

4) THE NORTHWEST

Interregional differences in the contrail-outbreak synoptic climatology for the Midwest, Northeast, and Southeast are relatively small; however, they show greater differences from the Northwest region. Accordingly, we present the synoptic climatology for this region. Although the atmospheric composites accompanying contrail outbreaks for the Northwest confirm positive pressure/height anomalies (ridging) in the troposphere (Fig. 8a), the placement of features is different from the eastern regions of contrail outbreak higher frequencies: geopotential height anomalies are most positive over the interior, decreasing to the northwest;

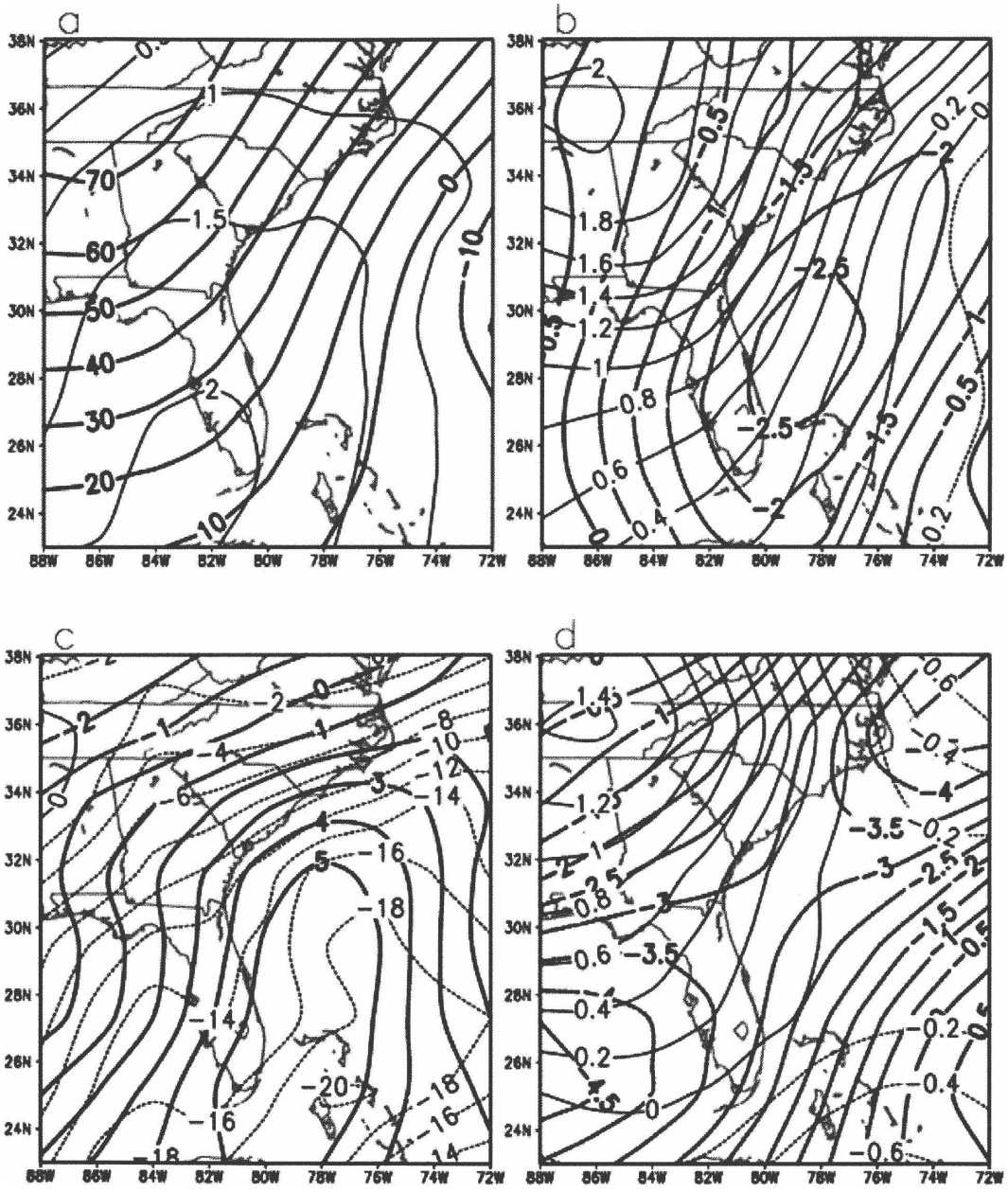

FIG. 7. Similar to Fig. 6, but for the Southeast (n = 38).

essentially the opposite pattern to that found for the eastern U.S. regions. These pressure/height anomaly patterns also differ from those for contrail outbreaks in the adjacent south subregions comprising California and Nevada (not shown), which show broadly similar anomaly patterns to those in eastern regions (e.g., warm-cored high pressure, meridional gradients of UT omega and humidity that comprise ascending air and increasing moisture to the west, in advance of a trough).

Temperature anomalies in the middle and upper troposphere for the Northwest are most positive to the south and east—accompanied by positive (southerly) wind components—suggesting more barotropic conditions attending contrail outbreaks here than for eastern regions (Figs. 8b,d). Sinking air in the ridge occurs over most of the Northwest (Fig. 8c), but with the strong gradients of vertical motion located south toward northern California, rather than to the northwest. Accordingly, the RH pattern in middle troposphere and UT (Fig. 8c) comprises negative anomalies over most of Washington but slightly positive anomalies over southern Oregon and northern California.

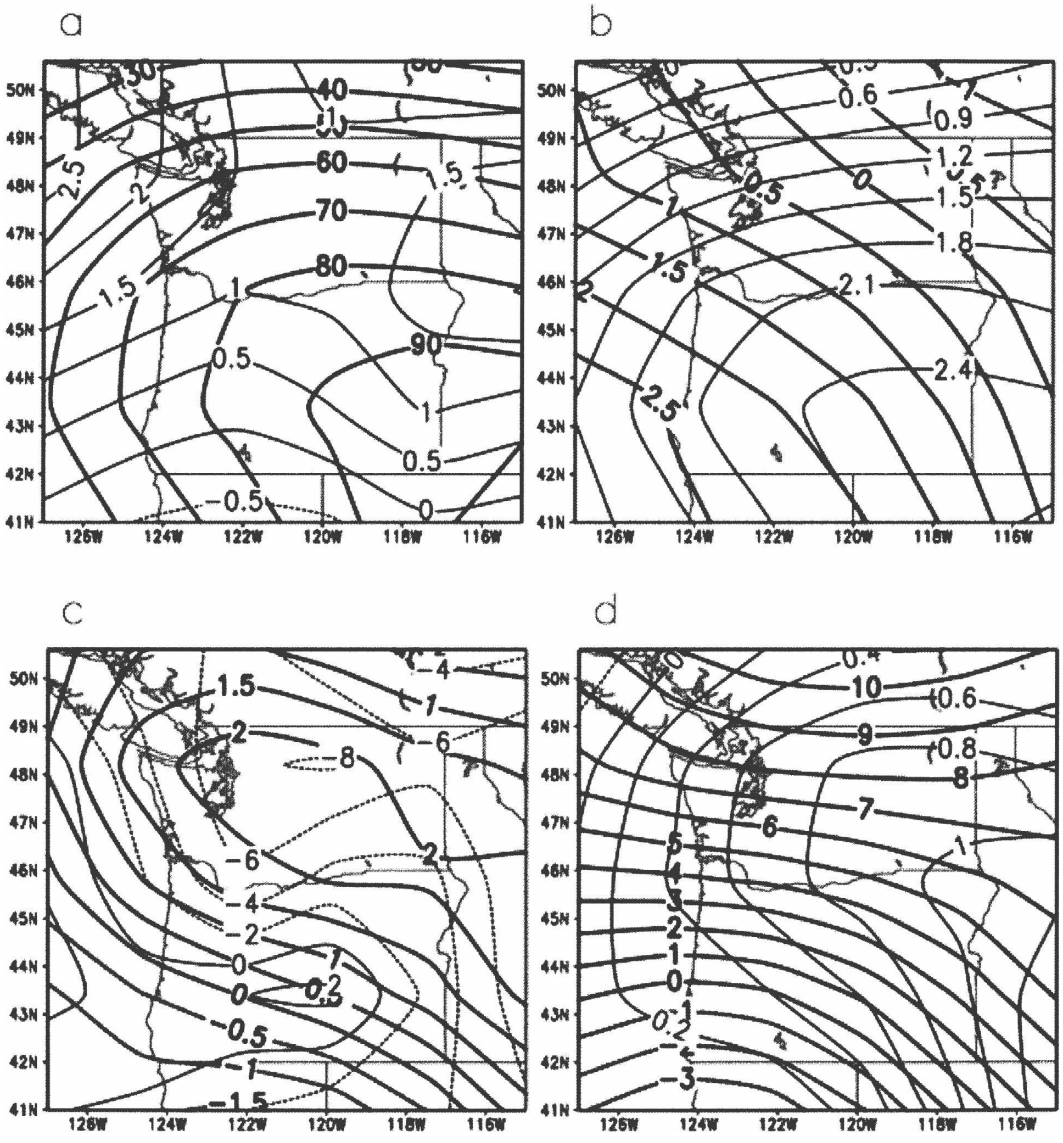

FIG. 8. Similar to Fig. 6, but for the Northwest ($n = 12$).

Contrail outbreaks in the Northwest have associated a particularly strong gradient of the UT u-wind anomaly (Fig. 8d), located between negative values over northern California and strongly positive values in British Columbia, Canada, which implies strong shear on the south side of the jet stream. Collectively, these composite anomaly patterns suggest that contrail outbreaks in clear or partly cloudy skies over the Northwest may be determined more by UT horizontal wind shear than by air rising over a wide area, in contrast to the eastern regions. If confirmed by subsequent analysis of additional years' satellite data (to increase the sample size) and/or the detailed investigation of contrail outbreak cases, this difference likely is explained by the Northwest's location, which more frequently places it beneath the jet stream, even in the warm season. Indeed, for the north-central and northwest United States, DeGrand et al. (2000, their Fig. 5) found maximum frequencies of contrails in July, rather than in the transition season months characteristic of the conterminous United States as a whole.

e. Climate diagnostics of contrail outbreaks and adjacent dense cirrus

In presenting the all-U.S. CDNs of contrail outbreaks for early–mid-September (1995–2001), our objectives are 1) to compare the synoptic climatology results obtained using the NNR daily-averaged data (section 4d)

TABLE 5. Composite area-weighted mean anomalies of NNR meteorological variables (i.e., CDNs) having significant differences* for contrail outbreaks ($n = 47$) and areas of thick cloud, including cirrus ($n = 20$), in early–mid-September periods of 1995–97 and 1999–2001.

Variable (level)	Contrail outbreak	Thick clouds	Two-tailed significance
RH (300)	+7.1%	+26.2%	0.000
SH (300)	$+0.417 \times 10^{-4}$ g kg^{-1}	$+2.387 \times 10^{-4}$ g kg^{-1}	0.000
dZ (300 – 200)	−6.5 m	+16.9 m	0.001
ω(200)	-5.1×10^{-5} hPa s^{-1}	-4.99×10^{-4} hPa s^{-1}	0.001
ω(250)	-5.4×10^{-5} hPa s^{-1}	-9.15×10^{-4} hPa s^{-1}	0.001
ω(300)	-2.5×10^{-5} hPa s^{-1}	-1.11×10^{-3} hPa s^{-1}	0.002
ω(300/250)	-4.5×10^{-5} hPa s^{-1}	-1.01×10^{-3} hPa s^{-1}	0.002
ω(300/200)	-4.9×10^{-5} hPa s^{-1}	-7.71×10^{-4} hPa s^{-1}	0.003
T (250)	−1.4°C	+0.4°C	0.005
du (200 – 250)	−0.5 m s^{-1}	+2.1 m s^{-1}	0.007
T (300)	−0.6°C	+1.5°C	0.01

* Equal to or less than the 0.01 probability level for a two-tailed Student's t test.

with the nonregional atmospheric composites of outbreaks derived using the 6-h data; and 2) to distinguish statistically the composite synoptic conditions of contrail outbreaks from those of thick clouds, including dense cirrus. Objective 2 is motivated by the observation (e.g., Fig. 1) that contrail outbreaks in otherwise clear or partly cloudy skies frequently occur downstream of the thick cirrus or multilayered clouds comprising fronts and jet streams.

Results evaluating the extent to which composite UT conditions associated with contrail outbreaks can be distinguished from those of dense cloud areas, mostly show statistical significance (Table 5): thick clouds, including cirrus, have associated greater moisture (both SH and RH), larger thickness (i.e., warmer air), stronger upward vertical motion, and stronger westerly winds (i.e., u-positive anomalies) relative to contrail outbreaks. The dense cirrus synoptic attributes are consistent with their frequent occurrence in and near the baroclinic zones accompanying upper troughs (e.g., Jasperson et al. 1985; Carlson 1991, chapter 12.3; Sassen and Campbell 2001; Mace et al. 2006); that is, a location to the west of most contrail outbreaks (Kästner et al. 1999). Because supersaturated air in the UT typically occurs downstream of the baroclinic zones comprising midlatitude storm tracks (Ludlam 1980; Detwiler and Pratt 1984; Spichtinger et al. 2003; Schumann 2005; Gettelman et al. 2006), contrail outbreaks develop preferentially within environments that are moistening, where the sign of the vertical motion changes from weakly subsiding to weakly ascending, and where the zonal wind and its associated horizontal shear increase. Accordingly, the contrail cirrus derived from outbreaks may help extend downstream the natural cirrus that develops from slantwise convection in baroclinic zones.

Clearly important for distinguishing contrail outbreak synoptic environments from those of thick clouds, including cirrus (Table 5), are the derived variables 300–200-hPa thickness [$Z(300) - Z(200)$] and the 250–200-hPa vertical shear of the u-wind, $u(200 – 250)$. These analyses may not always be available to a synoptician interested in short-term prediction of CFAs, even though forecast fields of humidity and cloud coverage at higher levels may be available (cf. NNR data). Accordingly, statistical correlation analysis indicates that the map of $T(250)$ substitutes for $Z(300 – 200)$—($r = 0.823$, $p < 0.01$)—a result expected from the hypsometric equation (Wallace and Hobbs 1977, chapters 2.2.2 and 2.2.3), and the $u(200)$ field alone can substitute for $u(200 – 250)$—($r = 0.344$, $p < 0.05$).

5. Summary and concluding remarks

The composite atmospheric environments (e.g., geopotential height, free-air temperature and thickness, vertical motion, humidity, wind) of contrail outbreaks occurring in otherwise clear or partly cloudy skies for the conterminous United States compose a regional synoptic climatology that emphasizes the dominant role of tropospheric synoptic patterns in their spatial and temporal variations. The mapped composites should permit identification operationally of the general areas prone to outbreaks. More precise delineation of CFAs at mesoscales and in real time could involve deriving additional explanatory variables, such as depth of the moist (supersaturated) layer, from a combination of ACARS data, rawinsonde ascents, and satellite data. Moreover, analyses such as these would permit an evaluation of the ability to hindcast contrail outbreaks from the occurrence of favored synoptic patterns identified in this study; similar to the retrodiction experiment undertaken for the aircraft grounding period of September 2001 (Travis et al. 2004).

Averaged for the United States, and for most of its subregions, contrail outbreaks are associated with the following generalized synoptic patterns and features: warm-cored high pressure (ridging); increased height of, and lowered temperature at, the tropopause; meridionally aligned strong gradients of vertical motion and UT humidity located between air that is rising and moist to the west—in advance of a trough—and sinking and dry to the east; and strengthening winds. Collectively, these imply a favored location for outbreaks between a ridge axis (to the east) and a trough (to the west), and near the forward edges of jet streams that accompany frontal systems located just upstream.

The synoptic climatology for those regions having higher frequencies of outbreaks and a generally greater contrail coverage factor—the Midwest, Northeast, and Southeast—indicates similarities in the associated synoptic conditions. However, geographic differences are evident in the relative importance of circulation controls for contrail outbreaks (e.g., land–sea contrasts in the Northeast), and from the inferred role of UT wind shear (the Northwest versus regions east of the Rocky Mountains). Given the strong similarities in contrail outbreak UT composites on synoptic and larger mesoscales (i.e., synoptic climatology, CDNs), there is no obvious disadvantage to our having used the NNR daily-averaged data to derive composite anomalies, rather than the 6-h maps. However, we emphasize the application here to spatial averaging of multiple events across time (i.e., generating regional-scale composite atmospheric fields of contrail outbreaks): the NNR 6-h data would be superior to the daily-averaged data for investigating an individual outbreak, yet even those data can be separated in time by up to 3 h with respect to the event.

The synoptic climatology of contrail outbreaks derived here can be compared and contrasted with other climatic studies, particularly those by Kästner et al. (1999) and Stuefer et al. (2005). In terms of the synoptic associations of contrails (e.g., gradually rising air accompanying divergence in the UT; moistening of air; horizontal shear), the present results for U.S. regions appear broadly similar to those derived for central Europe using a combination of observational data and mesoscale meteorological model output (Kästner et al. 1999). At the same time, the present results specifically are with regard to contrail outbreaks in otherwise clear or partly cloudy skies that are usually some distance downstream of frontal and jet stream locations; hence, these contrast with the stronger baroclinity found in the Kästner et al. (1999) study. Because the present analysis discloses contrail outbreak associated composite synoptic patterns derived primarily from observation data (i.e., NNR), it differs also from the contrail forecast method for Alaska that uses output from the fifth-generation Pennsylvania State University–National Center for Atmospheric Research Mesoscale Model (MM5; Stuefer et al. 2005). Even so, the ability to predict contrails over Fairbanks shows a similarly strong dependence on UT humidity and temperature. Moreover, the present regional-scale synoptic composites can be considered a necessary first step toward evaluating the predictability of contrail outbreaks using NWP fields for the conterminous United States (i.e., the "lower 48" states).

The CDNs for the early–mid-September period show statistically different synoptic environments of contrail outbreaks versus sample areas of dense clouds, including thick cirrus, from which physical differences are inferred. Typically, thick clouds and cirrus located upstream (i.e., west) of contrail outbreaks represent an intensification of the UT conditions associated with the persisting contrails composing outbreaks. This result supports a role for contrail outbreaks in helping to extend the spatial coverage of natural cirrus and cirrostratus (e.g., Mannstein and Schumann 2005), and may also explain why surface observations of multiple contrails at a location frequently precede significant precipitation by 12–24 h (e.g., Harami 1968). Accordingly, contrail outbreaks likely are involved in some high-cloud increases observed in recent decades for the United States and other regions, especially Europe and the North Pacific (e.g., Zerefos et al. 2003; Minnis et al. 2004, 2005; Stordal et al. 2005; Mannstein and Schumann 2005). The present analysis for midseason months of 2000–02 suggests an additional 2% cirrus cloud coverage in those regions (the Midwest, Northeast, and Southeast) having high frequencies of outbreaks due to jet air traffic (i.e., 7%–8% coverage by outbreaks assuming one-quarter sky coverage).

Globally, the frequencies of persisting contrails and outbreaks likely will increase as the number of jet planes and flights increase, and the opportunity for CFAs to be so transited also is increased. It is anticipated (Penner et al. 1999) that jet fuel consumption will increase at around +3% per year through at least 2015. This is somewhat less than the expected change in frequency of jet flights (+5%–6% per year), owing to improvements in engine performance and the use of fuels having different properties. Accordingly, studies project increasing frequencies of contrails along major long-haul flight paths, particularly outside the North America–Atlantic–Europe sector, that potentially would enhance the contrail role in future regional and even global-scale climate changes (Gierens et al. 1999; Minnis et al. 1999; Marquart et al. 2003). Realization of

these potential climatic impacts of contrails and outbreaks depends significantly upon the occurrence of favorable UT conditions associated with the synoptic atmospheric circulation.

Acknowledgments. This research was supported by NSF BCS Grants 0099014 and 0099011. We are grateful for the assistance of Steve Curran (The Pennsylvania State University) and Jeff Johnson (University of Wisconsin—Whitewater). The valuable comments by the three anonymous reviewers of this paper are greatly appreciated.

APPENDIX

Acronyms List

ACARS	Aircraft Communication, Addressing, and Reporting System
AVHRR	Advanced Very High Resolution Radiometer (NOAA)
CCF	Contrail coverage factor
CDNs	Climate diagnostics
CFA	Contrail favored area
DTR	Diurnal temperature range
GIS	Geographic information system
GCM	General circulation model
IR	(Thermal) infrared
MM5	Fifth-generation Pennsylvania State University–National Center for Atmospheric Research Mesoscale Model
NCEP–NCAR	National Centers for Environmental Prediction–National Center for Atmospheric Research
NNR	NCEP–NCAR reanalysis
NOAA	National Oceanic and Atmospheric Administration
NWP	Numerical weather prediction
RH	Relative humidity
SH	Specific humidity
UT	Upper troposphere
UTH	Upper-tropospheric humidity

REFERENCES

Angell, J. K., 1990: Variation in United States cloudiness and sunshine duration between 1950 and the drought year of 1988. *J. Climate,* **3,** 296–308.

Appleman, H., 1953: The formation of exhaust condensation trails by jet aircraft. *Bull. Amer. Meteor. Soc.,* **34,** 14–20.

Atlas, D., Z. Wang, and D. P. Duda, 2006: Contrails to cirrus—Morphology, microphysics, and radiative properties. *J. Appl. Meteor. Climatol.,* **45,** 5–19.

BACK Aviation Solutions, cited 2005: OAG schedules database, New Haven, CT. [Available online at http://www.backaviation.com/Information_Services/Products/schedules.htm.]

Bakan, S., M. Betancor, V. Gayler, and H. Grassl, 1994: Contrail frequency over Europe from NOAA-satellite images. *Ann. Geophys.,* **12,** 962–968.

Barry, R. G., 1970: A framework for climatological research with particular reference to scale concepts. *Trans. Inst. Brit. Geogr.,* **49,** 61–70.

——, and A. M. Carleton, 2001: *Synoptic and Dynamic Climatology*. Routledge, 620 pp.

Boucher, O., 1999: Air traffic may increase cirrus cloudiness. *Nature,* **397,** 30–31.

Busen, R., and U. Schumann, 1995: Visible contrail formation from fuels with different sulfur contents. *Geophys. Res. Lett.,* **22,** 1357–1360.

Businger, S., D. I. Knapp, and G. F. Watson, 1990: Storm following climatology of precipitation associated with winter cyclones originating over the Gulf of Mexico. *Wea. Forecasting,* **5,** 378–403.

Cardinali, C., L. Isaksen, and E. Andersson, 2003: Use and impact of automated aircraft data in a global 4DVAR data assimilation system. *Mon. Wea. Rev.,* **131,** 1865–1877.

Carleton, A. M., 1999: Methodology in climatology. *Ann. Assoc. Amer. Geogr.,* **89,** 713–735.

——, and P. J. Lamb, 1986: Jet contrails and cirrus cloud: A feasibility study employing high-resolution satellite imagery. *Bull. Amer. Meteor. Soc.,* **67,** 301–309.

Carlson, T. N., 1991: *Mid-Latitude Weather Systems*. HarperCollins Academic, 507 pp.

Changnon, S. A., 1981: Midwestern cloud, sunshine and temperature trends since 1901: Possible evidence of jet contrail effects. *J. Appl. Meteor.,* **20,** 496–508.

——, R. G. Semonin, and W. M. Wendland, 1980: Effect of contrail cirrus on surface weather conditions in the Midwest: Phase I. Illinois State Water Survey Final Rep. of NSF Grant ATM 78-09568, 141 pp. [Available from Atmospheric Sciences Division, Illinois State Water Survey, 2204 Griffith Dr., Champaign, IL 61820-7495.]

Chlond, A., 1998: Large-eddy simulation of contrails. *J. Atmos. Sci.,* **55,** 796–819.

Dee, D. P., and A. M. Da Silva, 2003: The choice of variable for atmospheric moisture analysis. *Mon. Wea. Rev.,* **131,** 155–171.

DeGrand, J. Q., A. M. Carleton, D. J. Travis, and P. J. Lamb, 2000: A satellite-based climatic description of jet aircraft contrails and associations with atmospheric conditions, 1977–79. *J. Appl. Meteor.,* **39,** 1434–1459.

Del Guasta, M., and E. Vallar, 2003: In-cloud variability of LIDAR depolarization of polar and midlatitude cirrus. *Geophys. Res. Lett.,* **30,** 1578, doi:10.1029/2003GL017163.

Detwiler, A., and H. Cho, 1982: Reduction of residential heating and cooling requirements possible through atmospheric seeding with ice-forming nuclei. *J. Appl. Meteor.,* **21,** 1045–1047.

——, and R. Pratt, 1984: Clear-air seeding: Opportunities and strategies. *J. Wea. Modif.,* **16,** 46–60.

Duda, D. P., J. D. Spinhirne, and W. D. Hart, 1998: Retrieval of contrail microphysical properties during SUCCESS by the split-window method. *Geophys. Res. Lett.,* **25,** 1149–1152.

——, P. Minnis, and L. Nguyen, 2001: Estimates of cloud radiative forcing in contrail clusters using GOES imagery. *J. Geophys. Res.,* **106** (D5), 4927–4938.

——, ——, ——, and R. Palikonda, 2004: A case study of the development of contrail clusters over the Great Lakes. *J. Atmos. Sci.,* **61,** 1132–1146.

——, ——, and R. Palikonda, 2005: Estimated contrail frequency and coverage over the contiguous United States from nu-

merical weather prediction analyses and flight track data. *Meteor. Z.,* **14,** 537–548.

Elliott, W. P., and D. J. Gaffen, 1991: On the utility of radiosonde humidity archives for climate studies. *Bull. Amer. Meteor. Soc.,* **72,** 1507–1520.

Engelstad, M., S. K. Sengupta, T. Lee, and R. M. Welch, 1992: Automated detection of jet contrails using the AVHRR split window. *Int. J. Remote Sens.,* **13,** 1391–1412.

Fichter, C., S. Marquart, R. Sausen, and D. S. Lee, 2005: The impact of cruise altitude on contrails and related radiative forcing. *Meteor. Z.,* **14,** 563–572.

Fortuin, J. P. F., R. Van Dorlund, W. M. F. Wauben, and H. Kelder, 1995: Greenhouse effects of aircraft emissions as calculated by a radiative transfer model. *Ann. Geophys.,* **13,** 413–418.

Freudenthaler, V., F. Homburg, and H. Jäger, 1995: Contrail observations by ground-based scanning lidar: Cross-sectional growth. *Geophys. Res. Lett.,* **22,** 3501–3504.

Garand, L., C. Grassotti, J. Halle, and G. L. Klein, 1992: On differences in radiosonde humidity-reporting practices and their implications for numerical weather prediction and remote sensing. *Bull. Amer. Meteor. Soc.,* **73,** 1417–1423.

Garber, D. P., P. Minnis, and P. K. Costulis, 2005: A commercial flight track database for upper tropospheric aircraft emission studies over the USA and southern Canada. *Meteor. Z.,* **14,** 445–452.

Gettelman, A., E. J. Fetzer, A. Eldering, and F. W. Irion, 2006: The global distribution of supersaturation in the upper troposphere from the Atmospheric Infrared Sounder. *J. Climate,* **19,** 6089–6103.

Gierens, K., 1996: Numerical simulations of persistent contrails. *J. Atmos. Sci.,* **53,** 3333–3348.

——, R. Sausen, and U. Schumann, 1999: A diagnostic study of the global distribution of contrails. Part II: Future air traffic scenarios. *Theor. Appl. Climatol.,* **63,** 1–9.

——, U. Schumann, M. Helten, H. Smit, and P.-H. Wang, 2000: Ice-supersaturated regions and subvisual cirrus in the northern midlatitude upper troposphere. *J. Geophys. Res.,* **105,** 22 743–22 753.

Gothe, M. B., and H. Grassl, 1993: Satellite remote sensing of the optical depth and mean crystal size of thin cirrus and contrails. *Theor. Appl. Climatol.,* **48,** 101–113.

Grassl, H., 1990: Possible climatic effects of contrails and additional water vapour. *Air Traffic and the Environment—Background, Tendencies and Potential Global Atmospheric Effects,* U. Schumann, Ed., Springer-Verlag, 124–137.

Hanson, H. M., and D. M. Hanson, 1995: A reexamination of the formation of exhaust condensation trails by jet aircraft. *J. Appl. Meteor.,* **34,** 2400–2405.

——, and ——, 1998: The application of the revised algorithm for the prediction of the formation of exhaust condensation trails by jet aircraft. *J. Appl. Meteor.,* **37,** 436–440.

Harami, K., 1968: Utilization of condensation trails for weather forecasting. *J. Meteor. Res. Japan,* **20,** 55–63.

Jackson, A., B. Newton, D. Hahn, and A. Bussey, 2001: Statistical contrail forecasting. *J. Appl. Meteor.,* **40,** 269–279.

Jasperson, W. H., G. D. Nastrom, R. E. Davis, and J. D. Holdeman, 1985: Variability of cloudiness at airline cruise altitudes from GASP measurements. *J. Climate Appl. Meteor.,* **24,** 74–82.

Jensen, E. J., A. S. Ackerman, D. E. Stevens, O. B. Toon, and P. Minnis, 1998: Spreading and growth of contrails in a sheared environment. *J. Geophys. Res.,* **103,** 31 557–31 567.

Kalnay, E., and Coauthors, 1996: The NCEP/NCAR 40-Year Reanalysis Project. *Bull. Amer. Meteor. Soc.,* **77,** 437–471.

Kästner, M., R. Meyer, and P. Wendling, 1999: Influence of weather conditions on the distribution of persistent contrails. *Meteor. Appl.,* **6,** 261–271.

Khvorostyanov, V., and K. Sassen, 1998: Cloud model simulation of a contrail case study: Surface cooling against upper tropospheric warming. *Geophys. Res. Lett.,* **25,** 2145–2148.

Kistler, R., and Coauthors, 2001: The NCEP–NCAR 50-Year Reanalysis: Monthly means CD-ROM and documentation. *Bull. Amer. Meteor. Soc.,* **82,** 247–267.

Kristensson, A., J.-F. Gayet, J. Strom, and F. Auriol, 2000: In situ observations of a reduction in effective crystal diameter in cirrus clouds near flight corridors. *Geophys. Res. Lett.,* **27,** 681–684.

Langford, A. O., R. W. Portmann, J. S. Daniel, H. L. Miller, C. S. Eubank, S. Solomon, and E. G. Dutton, 2005: Retrieval of ice crystal effective diameters from ground-based near-infrared spectra of optically thin cirrus. *J. Geophys. Res.,* **110,** D22201, doi:10.1029/2005JD005761.

Lee, J. E., and S. D. Johnson, 1985: Expectancy of cloudless photographic days in the contiguous United States. *Photogramm. Eng. Remote Sens.,* **51,** 1883–1891.

Lee, T. F., 1989: Jet contrail identification using the AVHRR infrared split window. *J. Appl. Meteor.,* **28,** 993–995.

Liepert, B. G., 1997: Recent changes in solar radiation under cloudy conditions in Germany. *Int. J. Climatol.,* **17,** 1581–1593.

Liou, K. N., 1992: *Radiation and Cloud Processes in the Atmosphere: Theory, Observation and Modeling*. Oxford University Press, 487 pp.

——, S. C. Ou, and G. Koenig, 1990: An investigation on the climatic effect of contrail cirrus. *Air Traffic and the Environment—Background, Tendencies and Potential Global Atmospheric Effects,* U. Schumann, Ed., Springer-Verlag, 154–169.

Ludlam, F. H., 1980: *Clouds and Storms: The Behavior and Effect of Water in the Atmosphere.* Pennsylvania State University Press, 405 pp.

Mace, G. G., S. Benson, and E. Vernon, 2006: Cirrus clouds and the large-scale atmospheric state: Relationships revealed by six years of ground-based data. *J. Climate,* **19,** 3257–3278.

Machta, L., and T. Carpenter, 1971: Trends in high cloudiness at Denver and Salt Lake City. *Man's Impact on the Environment,* W. H. Mathews, W. W. Kellogg, and G. D. Robinson, Eds., MIT Press, 410–415.

Mannstein, H., and U. Schumann, 2005: Aircraft induced contrail cirrus over Europe. *Meteor. Z.,* **14,** 549–554.

——, R. Meyer, and P. Wendling, 1999: Operational detection of contrails from NOAA-AVHRR data. *Int. J. Remote Sens.,* **20,** 1641–1660.

Marquart, S., M. Ponater, F. Mager, and R. Sausen, 2003: Future development of contrail cover, optical depth, and radiative forcing: Impacts of increasing air traffic and climate change. *J. Climate,* **16,** 2890–2904.

Martin, F. L., and V. V. Salomonson, 1970: Statistical characteristics of subtropical jet-stream features in terms of MRIR observations from Nimbus II. *J. Appl. Meteor.,* **9,** 508–520.

Matuszko, D., 2002: Long-term course of cloud genera frequency in Cracow (1906–2000). *Eos, Trans. Amer. Geophys. Union,* **83,** 528.

Meerkötter, R., U. Schumann, D. R. Doelling, P. Minnis, T. Nakajima, and Y. Tsushima, 1999: Radiative forcing by contrails. *Ann. Geophys.,* **17,** 1080–1094.

Meyer, R., H. Mannstein, R. Meerkötter, U. Shumann, and P. Wendling, 2002: Regional radiative forcing by line-shaped contrails derived from satellite data. *J. Geophys. Res.,* **107,** 4104, doi:10.1029/2001JD000426.

Miloshevich, L. M., H. Vömel, A. Paukkunen, A. J. Heymsfield, and S. J. Oltmans, 2001: Characterization and correction of relative humidity measurements from Vaisala RS80-A radiosondes at cold temperatures. *J. Atmos. Oceanic Technol.,* **18,** 135–156.

Minnis, P. J., D. F. Young, D. P. Garber, L. Nguyen, W. L. Smith Jr., and R. Palikonda, 1998: Transformation of contrails into cirrus during SUCCESS. *Geophys. Res. Lett.,* **25,** 1157–1160.

——, U. Schumann, D. R. Doelling, K. M. Gierens, and D. W. Fahey, 1999: Global distribution of contrail radiative forcing. *Geophys. Res. Lett.,* **26,** 1853–1856.

——, J. K. Ayers, M. L. Nordeen, and S. P. Weaver, 2003: Contrail frequency over the United States from surface observations. *J. Climate,* **16,** 3447–3462.

——, ——, ——, R. Palikonda, and D. Phan, 2004: Contrails, cirrus trends, and climate. *J. Climate,* **17,** 1671–1685.

——, R. Palikonda, B. J. Walter, J. K. Ayers, and H. Mannstein, 2005: Contrail properties over the eastern North Pacific from AVHRR data. *Meteor. Z.,* **14,** 515–523.

Moninger, W. R., R. D. Mamrosh, and P. M. Pauley, 2003: Automated meteorological reports from commercial aircraft. *Bull. Amer. Meteor. Soc.,* **84,** 203–216.

Moss, S. J., 1999: The testing and verification of contrail forecasts using pilot observations from aircraft. *Meteor. Appl.,* **6,** 193–200.

Myhre, G., and F. Stordal, 2001: On the tradeoff of the solar and thermal infrared radiative impact of contrails. *Geophys. Res. Lett.,* **28,** 3119–3122.

Nakanishi, S., J. Curtis, and G. Wendler, 2001: The influence of increased jet airline traffic on the amount of high level cloudiness in Alaska. *Theor. Appl. Climatol.,* **68,** 197–205.

Newton, B., A. Jackson, D. Hahn, and A. Bussey, 1997: Statistical contrail forecasting. Preprints, *Seventh Conf. on Aviation, Range, and Aerospace Meteorology,* Long Beach, CA, Amer. Meteor. Soc., 463–468.

Nicodemus, M. L., and J. D. McQuigg, 1969: A simulation model for studying possible modification of surface temperature. *J. Appl. Meteor.,* **8,** 199–204.

Ovarlez, J., P. Van Velthoven, G. Sachse, S. Vay, H. Schlager, and H. Ovarlez, 2000: Comparison of water vapor measurements from POLINAT 2 with ECMWF analyses in high-humidity conditions. *J. Geophys. Res.,* **105,** 3737–3744.

Palikonda, R., P. Minnis, P. K. Costulis, and D. P. Duda, 2002: Contrail climatology over the USA from MODIS and AVHRR data. Preprints, *10th Conf. on Aviation, Range, and Aerospace Meteorology,* Portland, OR, Amer. Meteor. Soc., J1.3.

——, ——, D. P. Duda, and H. Mannstein, 2005: Contrail coverage derived from 2001 AVHRR data over the continental United States of America and surrounding areas. *Meteor. Z.,* **14,** 525–536.

Penner, J. E., D. H. Lister, D. J. Griggs, D. J. Dokken, and M. McFarland, Eds., 1999: *Aviation and the Global Atmosphere*. Cambridge University Press, 373 pp.

Peters, J. L., 1993: New techniques for contrail forecasting. Air Weather Service Scott Air Force Base Tech. Rep. AWS/TR-93/001, AD-A269686, 31 pp.

Pielke, R. A., Sr., 2003: Heat storage within the Earth system. *Bull. Amer. Meteor. Soc.,* **84,** 331–335.

Pilié, R. J., and J. E. Jiusto, 1958: A laboratory study of contrails. *J. Meteor.,* **15,** 149–154.

Poellot, M. R., W. P. Arnott, and J. Hallett, 1999: In situ observations of contrail microphysics and implications for their radiative impact. *J. Geophys. Res.,* **104,** 12 077–12 084.

Ponater, M., S. Brinkop, R. Sausen, and U. Schumann, 1996: Simulating the global atmospheric response to aircraft water vapor emissions and contrails: A first approach using a GCM. *Ann. Geophys.,* **14,** 941–960.

——, S. Marquart, and R. Sausen, 2002: Contrails in a comprehensive global climate model: Parameterization and radiative forcing results. *J. Geophys. Res.,* **107,** 4164, doi:10.1029/2001JD000429.

——, ——, and ——, 2005: On contrail climate sensitivity. *Geophys. Res. Lett.,* **32,** L10706, doi:10.1029/2005GL022580.

Reichler, T., M. Dameris, and R. Sausen, 2003: Determining the tropopause height from gridded data. *Geophys. Res. Lett.,* **30,** 2042, doi:10.1029/2003GL018240.

Rind, D., P. Lonergan, and K. Shah, 1996: Climatic effect of water vapor release in the upper troposphere. *J. Geophys. Res.,* **101,** 29 395–29 405.

Roderick, M. L., and G. D. Farquhar, 2002: The cause of decreased pan evaporation over the past 50 years. *Science,* **298,** 1410–1411.

Ross, M. N., R. R. Friedl, D. E. Anderson, M. R. Berman, B. Gandrud, W. T. Rawlins, E. C. Richard, and A. F. Tuck, 1999: Study blazing new trails into effects of aviation and rocket exhaust in the atmosphere. *Eos, Trans. Amer. Geophys. Union,* **80,** 437, 442–443.

Ross, R. J., and W. P. Elliott, 2001: Radiosonde-based Northern Hemisphere tropospheric water vapor trends. *J. Climate,* **14,** 1602–1612.

Sassen, K., 1997: Contrail-cirrus and their potential for regional climate change. *Bull. Amer. Meteor. Soc.,* **78,** 1885–1903.

——, and J. R. Campbell, 2001: A midlatitude cirrus cloud climatology from the Facility for Atmospheric Remote Sensing. Part I: Macrophysical and synoptic properties. *J. Atmos. Sci.,* **58,** 481–496.

——, J. M. Comstock, Z. Wang, and G. G. Mace, 2001: Cloud and aerosol research capabilities at FARS: The Facility for Atmospheric Remote Sensing. *Bull. Amer. Meteor. Soc.,* **82,** 1119–1138.

Sausen, R., K. Gierens, M. Ponater, and U. Schumann, 1998: A diagnostic study of the global distribution of contrails. Part I: Present day climate. *Theor. Appl. Climatol.,* **61,** 127–141.

——, and Coauthors 2005: Aviation radiative forcing in 2000: An update on IPCC (1999). *Meteor. Z.,* **14,** 555–561.

Schrader, M. L., 1997: Calculations of aircraft contrail formation critical temperatures. *J. Appl. Meteor.,* **36,** 1725–1728.

Schröder, F., and Coauthors, 2000: On the transition of contrails into cirrus clouds. *J. Atmos. Sci.,* **57,** 464–480.

Schumann, U., 1996: On conditions for contrail formation from aircraft exhausts. *Meteor. Z.,* **5,** 4–23.

——, 2000: Influence of propulsion efficiency on contrail formation. *Aerosp. Sci. Technol.,* **4,** 391–401.

——, 2005: Formation, properties and climatic effects of contrails. *Comptes Rendus Phys.,* **6,** 549–565.

——, and P. Wendling, 1990: Determination of contrails from satellite data and observational results. *Air Traffic and the Environment—Background, Tendencies and Potential Global Atmospheric Effects,* U. Schumann, Ed., Springer-Verlag, 138–153.

——, J. Ström, R. Busen, R. Bauman, K. Gierens, M. Krautstrunk,

F. P. Schröder, and J. Sting, 1996: In situ observations of particles in jet aircraft exhausts and contrails for different sulfur-containing fuels. *J. Geophys. Res.,* **101,** 6853–6869.

Scorer, R. S., and L. J. Davenport, 1970: Contrails and aircraft downwash. *J. Fluid Mech.,* **43,** 451–464.

Seaver, W. L., and J. E. Lee, 1987: A statistical examination of sky cover changes in the contiguous United States. *J. Climate Appl. Meteor.,* **26,** 88–95.

Spichtinger, P., K. Gierens, and W. Read, 2003: The global distribution of ice-supersaturated regions as seen by the Microwave Limb Sounder. *Quart. J. Roy. Meteor. Soc.,* **129,** 3391–3410.

Stordal, F., G. Myhre, E. J. G. Stordal, W. B. Rossow, D. S. Lee, D. W. Arlander, and T. Svendby, 2005: Is there a trend in cirrus cloud cover due to aircraft traffic? *Atmos. Chem. Phys.,* **5,** 2155–2162.

Strauss, B., R. Meerkötter, B. Wissinger, P. Wendling, and M. Hess, 1997: On the regional climatic impact of contrails—Microphysical and radiative properties of contrails and cirrus. *Ann. Geophys.,* **15,** 1457–1467.

Stubenrauch, C. J., and U. Schumann, 2005: Impact of air traffic on cirrus coverage. *Geophys. Res. Lett.,* **32,** L14813, doi:10.1029/2005GL022707.

Stuber, N., P. Forster, G. Rädel, and K. Shine, 2006: The importance of the diurnal and annual cycle of air traffic for contrail radiative forcing. *Nature,* **441,** 864–867.

Stuefer, M., X. Meng, and G. Wendler, 2005: MM5 contrail forecasting in Alaska. *Mon. Wea. Rev.,* **133,** 3517–3526.

Sun, B., and P. Ya Groisman, 2004: Variations in low cloud cover over the United States during the second half of the twentieth century. *J. Climate,* **17,** 1883–1888.

Travis, D. J., 1996a: Variations in contrail morphology and relationships to atmospheric conditions. *J. Wea. Modif.,* **28,** 50–58.

——, 1996b: Diurnal temperature range modifications induced by contrails. Preprints, *13th Conf. on Planned and Inadvertent Weather Modification,* Atlanta, GA, Amer. Meteor. Soc., 110–111.

——, and S. A. Changnon, 1997: Evidence of jet contrail influences on regional-scale diurnal temperature range. *J. Wea. Modif.,* **29,** 74–83.

——, and A. M. Carleton, 2005: Characteristics of jet contrail increases and implications on aviation policy decision-making. Preprints, *15th Conf. on Applied Climatology,* Savannah, GA, Amer. Meteor. Soc., JP 2.6.

——, A. M. Carleton, and S. A. Changnon, 1997: An empirical model to predict widespread occurrences of contrails. *J. Appl. Meteor.,* **36,** 1211–1220.

——, ——, and R. G. Lauritsen, 2002: Contrails reduce daily temperature range. *Nature,* **418,** 601.

——, ——, and ——, 2004: Regional variations in U.S. diurnal temperature range for the 11–14 September 2001 aircraft groundings: Evidence of jet contrail influence on climate. *J. Climate,* **17,** 1123–1134.

——, ——, J. S. Johnson, and J. Q. DeGrand, 2007: U.S. jet contrail frequency changes: Influences of jet aircraft flight activity and atmospheric conditions. *Int. J. Climatol.,* **27,** 621–632.

Vay, S. A., and Coauthors, 2000: Tropospheric water vapor measurements over the North Atlantic during the Subsonic Assessment Ozone and Nitrogen Oxide Experiment (SONEX). *J. Geophys. Res.,* **105,** 3745–3756.

Wallace, J. M., and P. V. Hobbs, 1977: *Atmospheric Science: An Introductory Survey*. Academic Press, 467 pp.

Williams, V., R. B. Noland, and R. Toumi, 2003: Air transport cruise altitude restrictions to minimize contrail formation. *Climate Policy,* **3,** 207–219.

Wylie, D., D. L. Jackson, W. P. Menzel, and J. J. Bates, 2005: Trends in global cloud cover in two decades of HIRS observations. *J. Climate,* **18,** 3021–3031.

Zerefos, C. S., K. Eleftheratos, D. S. Balis, P. Zanis, G. Tselioudis, and C. Meleti, 2003: Evidence of impact of aviation on cirrus cloud formation. *Atmos. Chem. Phys.,* **3,** 1633–1644.